

# Optimizing the Automated Assembly Process for Filled-Polymer Based Thermal Bondlines

David F. Rae<sup>1,2,4</sup>, Peter Borgesen Ph.D.<sup>1,3</sup>

<sup>1</sup>Unovis Solutions, P.O. Box 5304, Binghamton, NY 13905

Eric Cotts Ph.D.<sup>2</sup>

<sup>2</sup>Materials Science Program and Department of Physics, Binghamton University,  
Binghamton, NY 13902

<sup>3</sup>Department of Systems Science & Industrial Engineering, Binghamton University,  
Binghamton, NY 13902

<sup>4</sup>Email: rae@unovis-solutions.com

## Abstract

Great efforts are expended by researchers to develop new and better thermal interface materials. In contrast, optimization of the performance of a given material is usually left to more empirical efforts. Unfortunately, interactions between the many parameters affecting performance make the design of experiments required for empirical optimization impractically large. We are conducting systematic mechanistic studies on the combined effects of materials selection and process parameters such as normal forces, assembly speeds, and thermal profiles on bondline macro/microstructure and thermal performance.

The most common type of medium/high-performance thermal interface material is undoubtedly that of polymers filled with conductive particles, most often Ag. However, these materials rarely perform as well in a practical application as predicted based on manufacturer supplied data sheets. This is usually ascribed to defects such as voids, porosity and filler distribution heterogeneity. Such defects can be minimized by process optimization, but we also believe that we can learn to tailor some level of heterogeneity to our advantage. In fact, a thermal resistance two and a half times lower than that predicted based on the data sheet has already been demonstrated for one high-end commercial material. Moreover, this can be compatible with a practical manufacturing process.

The present paper offers a discussion of results of systematic process studies on commercial filled polymer materials, including correlations between process parameters, defects and final bondline thickness. Important insights were derived from a new technique allowing the in-situ measurement of bondline electrical resistance during processing. The indication is that the dominant pathways for heat transport are provided by chains of Ag particles in good electrical contact with each other. However, typical thermal conductivities of adhesives with, say, 30% Ag (by volume) are lower than that of pure Ag by a factor of fifty or more. The reason for this is that a relatively small fraction of the Ag particles are in conducting chains; in many instances heat must travel through interfaces between the Ag and thin coatings or layers of polymer. Indications are that the fraction of metallic (electron) transport (transport through chains of Ag) can be enhanced in an optimized assembly process.

## Introduction

Thermal interface materials (TIMs) improve the efficiency of heat transfer in gaps between imperfectly matching components by displacing air, a poor heat transfer medium. Filled-polymer based systems are one widely-used and high-performance class of TIM. The solid fill serves to increase the thermal conductivity of the composite while the polymer provides a carrier matrix for the filler particles during processing. When the polymer component is cross-linked after pressing a TIM deposit between the components, the thin region (15-200  $\mu\text{m}$ ) between the components surfaces is referred to as a thermal bondline. The final macro and microstructure of this region dictates the thermal performance of the bondline. As this structure is highly process dependent, it is necessary to control the three stages of bondline assembly; these stages being: 1) material deposition; 2) bondline formation; 3) bondline structure stabilization (through mechanical means and/or curing reaction). One of the usual goals in industry is a bondline macrostructure with a homogeneous lateral distribution of solid filler across the bondline area.

Creating a thermal bondline that has a laterally homogeneous filler distribution over the component area using a well-designed off-the-shelf viscous TIM is generally straight-forward, an example of such a bondline is shown in Fig. 1a. However, such a bondline macrostructure does not guarantee bulk material microstructure or performance characteristics. Especially for TIMs fabricated with platelet or rod shaped filler particles, there is an opportunity for reorientation of the particles in the matrix during the squeeze-flow bondline formation process. This is due to the shear-rate gradients that evolve as the material spreads to cover the bondline area, particle-particle, and/or particle-component surface interactions. Furthermore, there is the possibility of defect introduction during assembly operations that can include voiding (gaseous phase inclusions) and/or delamination, flow-induced particle-depleted regions, or a poorly selected cure or post bondline

formation heat treatment which may alter the intrinsic structure of the matrix material. Due to such factors, the thermal resistance of a bondline ( $R_b$ ) is generally measured to be poorer than would be predicted from the manufacturer data sheet values by the equation:

$$R_b = \frac{H}{\lambda_{TIM}} \quad (1)$$

where  $H$  is the bondline thickness (15-100  $\mu\text{m}$  is usual) and  $\lambda_{TIM}$  is the thermal conductivity of the TIM as measured for an unconstrained bulk sample. Consequently, an expression such as

$$R_b = \frac{H}{\lambda_{eff}} + R_d + R_{c1} + R_{c2} \quad (2)$$

is more useful, where  $\lambda_{TIM}$  is replaced with an effective thermal conductivity of the TIM ( $\lambda_{TIM}$ ) in a bondline configuration.  $R_d$  is the additional thermal resistance associated with defects in the bondline matrix, with  $R_{c1}$  and  $R_{c2}$  representing the contact resistances due to material mismatches between the TIM and the component surfaces.

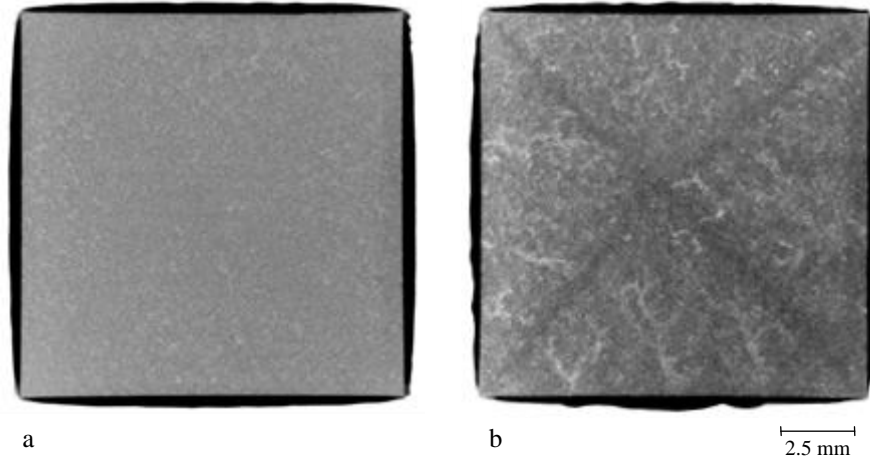


**Fig. 1. X-ray images of silver-flake filled polymer based TIM bondlines prepared between two pieces of double-side polished Si using a process that generated two very different bondline macrostructures: (a) laterally homogeneous; (b) laterally heterogeneous. The dark, silver-rich X pattern of (b) largely follows the illustration of Fig. 2b, with light tributary-like silver-poor zones situated between stagnant-flow locations.**

While bondlines created with a laterally homogeneous filler distribution are common in industry and the laboratory setting, bondlines that have significant filler distribution heterogeneity are not unusual, for example Fig. 1b and [1]. The factors associated with this behavior are related to the TIM formulation, component surface morphology and material properties, as well as the bondline formation process. Such heterogeneity, as discussed in this work, is due to particle entrapment and fluid exclusion that create filler compaction in low shear rate regions; several examples of such stagnant zones observed in squeeze flows are included in Fig. 2. As the composite's polymeric matrix fluid is excluded near these stagnant zones the filler density fraction increases in the adjacent region and reduced filler density fraction regions are created as the excluded matrix fluid moves to the perimeter of the bondline area, Fig. 1b and in [1].

Exploitation of such heterogeneous compaction zones can be expected to provide substantial improvements to heat transfer across the bondline as compared to those with prepared with homogeneous lateral filler distributions. This is due to the compacted filler-rich regions, which provide a second and markedly more efficient heat flow path than through the bulk TIM. For example, one of the TIMs evaluated in [1] was composed of 20% silver-flake filler by volume surrounded by an epoxy matrix. Assuming all of the silver filler to be contained in solid columns extending across the bondlines, cf. Fig. 3b, the effective thermal conductivity of the material in bondline configuration ( $\lambda_b$ ) would be 86 W/mK, see the following theory section for further discussion on this calculated value. In contrast, the unconstrained bulk  $\lambda_{TIM}$  was measured to be 2.1% of this potential value, or less than 2 W/mK [1].

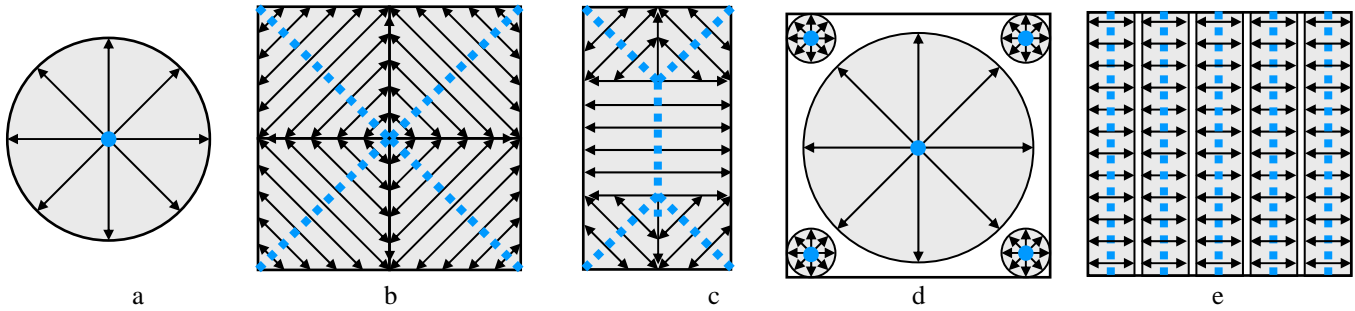


**Fig. 2. Illustrations of stagnant-flow locations (indicated as a dot or dashed line) developed in squeeze-flow bondline formation. Arrows indicate general flow directions during squeeze-flow bondline formation, are approximate, and do not indicate flow velocity. For (a-c) the bondline area between components is considered to be fully filled with TIM (shaded regions) for several substrate geometries: (a) disk; (b) square; (c) rectangle. For (d-e), a partially filled bondline area is considered, where the material deposit pattern was composed of several initial deposits: (d) 5 dots; (e) 5 rectangles. In (d-e) the squeeze flow bondline process is understood to be in progress, leading to multiple stagnant flow locations that develop prior to full coverage of the bondline area by the TIM.**

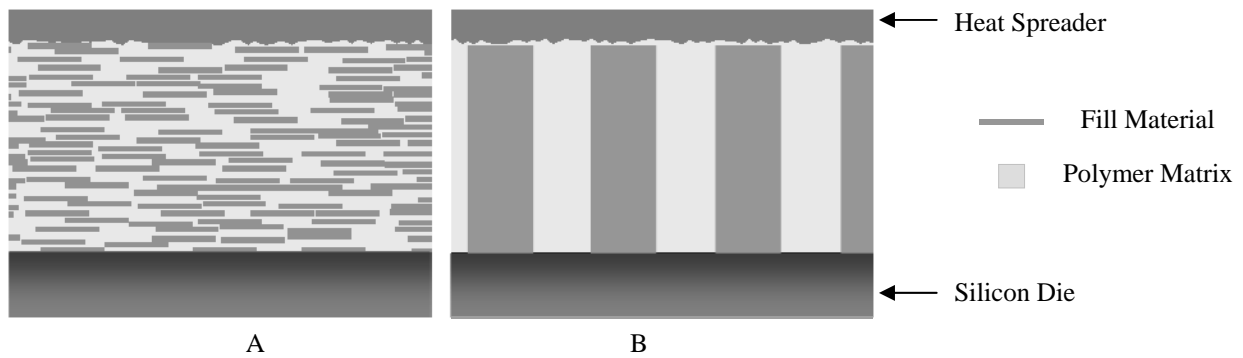


**Fig. 3. Schematic of filler distribution across the bondline thickness with a: (a) nominally homogeneous and random lateral filler distribution; (b) heterogeneous lateral filler distribution that can be modeled thermal resistance elements in parallel, Eqs.5-6. The filler area fraction ( $X_f=0.2$ ) and particle size between figures (a) and (b) are constant.**

In order to realize this improved  $\lambda_b$  for a given material, flow-induced heterogeneity can be used to increase the compacted area fraction of the bondline to approach the microstructure of Fig. 3b. Given a TIM prone to flow induced phase separation and compaction, there are two complimentary approaches possible: 1) optimization of the material deposition pattern; 2) optimization of the bondline formation process. To increase the area of the compacted filler regions in the final bondline, the TIM deposit pattern can be selected to increase the total length of the stagnant flow zone. It is around these regions that flow induced heterogeneity and compaction initiates during squeeze-flow bondline formation. One such modified pattern is shown during mid squeeze by Fig. 2e. By depositing material centered along the 5 dashed lines of Fig. 2e, the total length of stagnant flow zone increases by a factor of 1.7 compared to the “X” shaped pattern of Fig. 2b. Further pattern modification to 30 linear deposits (as used in this work) provides a factor of 10.6 increase. An additional benefit of this pattern is that during the squeeze-flow bondline formation, air and then matrix material displaced during compaction can readily escape to the perimeter of the bondline area through the channels between the stagnant flow regions. During the squeeze-flow bondline formation, process variables that can effect filler compaction include: movement speeds and path; normal forces applied; temperature profile. The relationship between these process variables and the onset of heterogeneity and compaction are discussed in the following theory section.

In this work, the results of processing on the bondline structure and resulting thermal and electrical properties were studied to identify methods to create improved thermal bondlines from commercially available TIMs. To understand the flow behavior of such materials, a TIM was characterized using steady rotation rheometry. The results of this characterization work was then used to compare experimental force vs. gap data collected during bondline formation to a literature model for squeezing

flows. Deviations from expected behavior can be attributed to onset of flow induced heterogeneity followed by compaction in the bondline.

The thermal performance of laterally homogeneous and heterogeneous bondlines prepared between copper coupons were measured with a flash thermal diffusivity method. The stability of bondline structure immediately after bondline formation was monitored using the electrical resistance of the bondline.

## Theory

### 1. Exploitation of Laterally Heterogeneous Compaction Zones to Improve Bondline Thermal Performance

The basis for Eq.1 is Fourier's law of heat transfer applied to the case of steady heat flow ( $\dot{Q}$ ) through the bondline with, no lateral temperature gradients over the hot and cool faces of the bondline, and adiabatic boundary conditions at the perimeter of the bondline. With these conditions, the temperature drop from the hot to the cool face of the bondline ( $\Delta T$ ) is constant across the bondline area ( $A_b$ ):

$$\dot{Q} = -\frac{\lambda_{TIM} A_b}{H} \Delta T \quad (3)$$

and an expression in terms of a heat flux ( $q$ ) is obtained by dividing by  $A_b$ :

$$q = \frac{\dot{Q}}{A_b} = -\frac{\lambda_{TIM}}{H} \Delta T = -\frac{\Delta T}{R_b} \quad (4)$$

which after rearrangement gives Eq.1.

By expanding Eq.3, an expression for the potential thermal conductivity ( $\lambda_b$ ) of a fully compacted structure segregated into areas of pure fill ( $A_f$ ) and pure matrix ( $A_m$ ), cf. Fig. 3b, is obtained:

$$\dot{Q} = -\frac{\lambda_b A_b}{H} \Delta T = -\frac{\lambda_f A_f}{H} \Delta T - \frac{\lambda_m A_m}{H} \Delta T \quad (5)$$

where  $\lambda_b$  is a function of the filler thermal conductivity ( $\lambda_f$ ) and matrix thermal conductivity ( $\lambda_m$ ). The above is in the form of resistance elements in parallel. This formulation again assumes no lateral temperature gradients across the substrate bondline interface. This may be approached in application by either a highly efficient heat spreader or finely distributed compaction regions. Dividing through by the constants gives:

$$\lambda_b = \left(\frac{A_f}{A_b}\right) \lambda_f + \left(\frac{A_m}{A_b}\right) \lambda_m \quad (6)$$

where the area fraction is equivalent to the volumetric fraction of the constituent filler. The value of 86 W/mK for TIM 1 at 20% silver fill by volume loading was calculated with the above, considering  $\lambda_f = 429$  W/mK [2] and  $\lambda_m = 0.2$  W/mK [1].

### 2. Bondline Formation

The most common method of bondline formation for a viscous TIM is through use of a squeeze-flow process. Material deposited onto one of the component surfaces is deformed when the other component is pressed into that deposit causing the TIM to flow between the approaching surfaces to the perimeter of the bondline area. Squeeze-flow has been an active field of research for well over a century due to its industrial importance. A recent review of the literature is available in [3].

With a TIM that matches a known rheological constitutive model, it is possible to monitor the bondline formation process for deviations from the expected behavior. Selection of an appropriate squeeze-flow model requires rheological characterization. For a simple Newtonian fluid, such as water, the ratio of shear stress ( $\tau$ ), to shear rate ( $\dot{\gamma}$ ) is a constant, referred to as the fluid's viscosity ( $\eta$ ). For filled polymers, this relationship is usually not applicable. However, over a limited range of shear-rate values and flow conditions, it may be possible to model filled TIM systems as power-law fluids:

$$\tau = \mathcal{A} \dot{\gamma}^n \quad (7)$$

where  $\tau$  is a function of consistency ( $\mathcal{A}$ ) and  $\dot{\gamma}$  raised to the flow behavior rate index ( $n$ ). This relationship can be also be discussed in terms of an effective shear viscosity ( $\eta_{eff}$ ) by dividing the shear stress by shear rate to obtained Eq.8.

$$\eta_{eff} = \frac{\tau}{\dot{\gamma}} = \mathcal{A}\dot{\gamma}^{n-1} \quad (8)$$

The simplest and most widely studied squeeze-flow configuration is that of the axisymmetric flow out of a central deposit, where a single deposit is placed between two approaching flat surfaces. The gap width ( $H$ ) is taken to be uniform between the surfaces. Given a Newtonian or power-law fluid and a no-slip boundary condition, the Scott equation [4] can be used:

$$F = \frac{-\dot{h}^n}{H^{2n+1}} \left( \frac{2n+1}{n} \right)^n \frac{2\pi \mathcal{A} R^{n+3}}{n+3} \quad (9)$$

where the normal force ( $F$ ) that arises due to the fluids resistance to flow is taken to be a function the power-law rheological model parameters in addition to the  $H$ , squeeze rate ( $\dot{h}$  or  $\partial H / \partial t$ ), and the cylindrical radius of the fluid confined between the surfaces ( $R$ ). This model also may be used with a Newtonian fluid where  $n=1$  and  $\mathcal{A} = \eta$ . This model is accurate at small gap widths where  $H/R \ll 1$  where the normal force developed is dominated by shear, rather than extensional flows [4]. Laun et al. expanded this analytical model to include wall slip phenomena [5].

Deviation from the squeeze-flow behavior predicted by Eq.9 towards normal forces larger than would be expected for a given gap condition have been found to indicate the onset of flow induced heterogeneity and compaction in TIM bondlines [1]. The onset of matrix-fluid migration from the stagnant flow locations during compaction in axisymmetric flows of paste-like materials has been studied and scaling arguments made in the rheology literature [6-8]. One such scaling argument proposed by [6] and reiterated in the form of Eq.10 by [8] defined a characteristic time for deformation of the composite material over the gap width ( $\tau_s$ ) and a characteristic time for the flow of the matrix fluid through the porous filler particle network of the composite over the gap width ( $\tau_m$ ). The ratio between these quantities, formalized as a Peclet number ( $Pe$ ), can be used to predict the most likely behavior, where  $Pe \ll 1$  would indicate the onset of self-filtration and compaction. For a power-law composite fluid in squeeze flow:

$$Pe = \frac{\tau_m}{\tau_s} = \frac{\eta_m \dot{h}^{1-n} H^{n+1}}{\mathcal{A} k} \quad (10)$$

where:  $\eta_w$  = matrix fluid viscosity  
 $\dot{h}$  = axial squeeze rate  
 $H$  = gap width  
 $\mathcal{A}$  = composite consistency  
 $n$  = composite flow rate index  
 $k$  = Darcy's permeability

and a critical squeeze rate ( $\dot{h}c$ ) corresponding to  $Pe = 1$  could then be identified [8].

$$\dot{h}c = \left( \frac{\mathcal{A} k}{\eta_m H^{n+1}} \right)^{\frac{1}{1-n}} \quad (11)$$

Notable, by inserting Eq.11 into Eq.9, a critical force ( $Fc$ ) can calculated for the gap conditions at which compaction will initiate.

$$Fc = \frac{-\dot{h}c^n}{H^{2n+1}} \left( \frac{2n+1}{n} \right)^n \frac{2\pi \mathcal{A} R^{n+3}}{n+3} \quad (12)$$

Once heterogeneity is prompted, increased normal force applied would be expected to compact the portion of the particle network entrapped between the substrates resulting in exclusion of matrix fluid and consolidation of the filler network.

From this discussion, two methods to prompt compaction would be to use either a relatively slow squeeze rate or low force during assembly, the result being a slow squeeze rate stage at some point in the bondline formation. The squeeze rate or force required to prompt compaction can be controlled through material selection. For example, to shift the onset of compaction to faster squeeze rates or higher applied normal forces, the matrix viscosity can be reduced or the permeability increased by use of larger filler particles that create larger pore volumes. Furthermore, as the rheology of many polymeric systems are strongly dependent on temperature, application of a heat source during bondline formation may also be used to modify the rheology of the composite. Past experience has shown that use of a slow squeeze rate is a quite efficient method to prompt compaction zones in the bondline [1].

## **Experimental Details**

### **1. Materials Examined**

Two commercially available TIM materials are discussed in this work:

- TIM 1 is composed of a two-part epoxy and silver flakes with a maximum long dimension of 45  $\mu\text{m}$  and thickness on the order of 5  $\mu\text{m}$ . According to the manufacturer-supplied technical data sheet, the material has a bulk conductivity of 2.5 W/mK. The silver content was 70% by weight as determined by thermogravimetric analysis (TGA). This value corresponds to approximately 20% by volume.
- TIM 2 is composed of a one part adhesive and silver flake fill. According to the manufacturer-supplied technical data sheet, the material has a bulk thermal conductivity of 11.3 W/mK. The silver content was 80% by weight as estimated by density measurement. This value corresponds to approximately 30% by volume.

### **2. Rheological Characterization**

A stress-controlled torsional rheometer was used to study the flow behavior of the thermal interface material in its uncured state (TA Instruments, AR-G2). Steel parallel plates with 25 mm diameter were used. Two surface finishes were used in the experiments. The surface was either a relatively smooth machined surface or roughened by attaching two self-adhesive abrasive disks to the parallel plate faces. Abrasive disks were cut from Buehler CarbiMet PSA backed 800 grit paper.

To load the sample, material was dispensed from a 3 ml syringe onto the lower plate. The upper plate was then brought into contact with the material and squeezed until the gap was fully filled. The edges were trimmed and outer surface cleaned with a lint free wipe before lowering the upper plate to create a slightly bowed out free surface. Several gap width values were used to visualize the influence of wall slip.

In test, a steady rotation strain rate sweep mode was used to investigate the flow behavior of the material. The shear rate was ramped from 0.01 to 10 1/s with 3 minutes allowed at each shear rate data point for the flows to approach steady flow condition. The condition of the sample in the gap was examined in-situ for edge instability at the free surface at high shear rates using the rheometer's built in camera. Data where edge instability occurred were removed from consideration.

### **3. Trilayer Bondline Assembly**

#### ***Substrates Used***

In this work, bondline samples were prepared in trilayer format with the TIM bondline existing between two substrate coupons; three types of coupon styles were used:

- Glass substrates were scribed and broken from microscope slides. Sample coupons described as rough were glass slides possessing 1 frosted side with a nominal average roughness of between 2-3  $\mu\text{m}$  as measured with a white light interferometer (Veeco, Wyko NT1100). Rough surfaces faced the TIM. Samples described as smooth were optically smooth glass microscope slides. Thickness was nominally 1 mm.
- Copper Substrate 1: Substrates were prepared from a nickel coated copper heat spreader using electrical discharge machining (EDM). Nickel was etched off using 3.75 M nitric acid at 55°C and rinsed with distilled water. Coupons were nominally 13.3 mm squares with a thickness of 0.48 mm.
- Copper Substrate 2: Copper substrates were prepared from an alloy 110 copper sheet with a #8 finish on one surface (McMaster-Carr, P/N 9821K12). Coupons were cut out using EDM and cleaned by swabbing the surfaces with copper cleaner (Kester #5520 Copper-Nu) before rinse with distilled water. Coupons were squares or disks with a nominal characteristic length of 12.7 mm and thickness of 1 mm.

### ***Material Deposition***

Several material deposition methods were used to fabricate the bondlines described in this work:

- Method 1: Manual syringe dispense of a single conical deposit onto the center of the lower substrate.
- Method 2: Automated dispense of 5 conical deposits onto the lower square substrate (Asymtek, Century 720, DV6322 auger pump, EFD 22 gauge tapered plastic tip). The center deposit was large relative to the peripheral four deposits located towards the corners of the substrate, similar to the pattern shown in Fig. 2d.
- Method 3: Manual stencil print with a 76.2  $\mu\text{m}$  thick electroformed stencil with 30 rectangular linear apertures, similar to the pattern shown in Fig. 2e. Stencil apertures were filled with single-sided razor blade squeegee.

### ***Assembly***

Approach 1: Bondline sample formation between substrates was carried out in a strain-controlled rheometer (TA Instruments, ARES) with custom fixturing. During assembly, a data acquisition system (Measurement Computing, USB-1608FS) concurrently collected normal force data from the rheometer's analog output port and gap width from two linear variable differential transformers (LVDTs) (Schaevitz MHR100 LVDT and ATA 2001 signal amplifier,). The LVDTs were located on either side of the sample during assembly. Vacuum ports were used to secure the substrates during assembly. Bondline samples were cured without an applied compressive load in a box oven.

Approach 2: Bondline sample formation between substrates occurred between two pistons within a bronze alignment sleeve. Upper and lower pistons with vacuum hold down ports were used to secure sample substrates. Motion of the upper piston relative to the lower piston was controlled by Instron Universal Testing Machine (Instron, 5500R). Bondline samples were cured without an applied compressive load in a box oven.

Approach 3: Bondline sample formation between substrates occurred in a fixture designed to apply a compressive load uniformly over the bondline area through a self leveling feature. The lower sample support was a surface ground stainless steel plate that rested on a bearing ball sectioned at the equator with a surface-ground flat surface. Positioned above this feature was an upper surface-ground stainless steel plate. The motion and load applied to the bondline through this plate was controlled by a pneumatic actuator attached to a vertically oriented linear slide attached to the Instron. The final load was controlled by regulating the air pressure applied to the air cylinder piston and the motion was controlled by coupling the mobile feature of the linear slide to the cross head mounted load cell via gimbal couple (1 kN Static Load Cell, Instron 2518-806). After assembly, the gap condition was maintained through 4 bolts that attached the upper plate to the lower plate. Bolts were tightened by hand at the end of the assembly while the ultimate force was applied. Bondline samples were cured under this nominal load in a box oven.

Approach 4: Bondline samples were formed using custom fixturing within the Instron. A support plate was attached to a cross head mounted load cell (1 kN Static Load Cell, Instron 2518-806) using a gimbal feature. A lower plate rested on the base of the tool. Substrates were attached to the upper plate by Kapton tape. After assembly, the gap condition was maintained through 4 bolts that attached the upper plate to the lower plate. Bolts were tightened by hand at the end of the assembly while the ultimate force was applied prior. Bondline samples were cured under this nominal load in a box oven. This approach was the basis for the fixture design discussed in Approach 3 above.

Approach 5: Bondline samples were formed within a bronze alignment sleeve between an upper piston and lower support. This lower sample support was a bearing ball sectioned at the equator with a ground flat surface. This feature was chosen to accommodate substrates that were not uniformly thick. The upper piston was attached to a pneumatic air cylinder that was used to apply a load to the sample located between the surfaces. Substrates were secured by vacuum ports present on both the upper piston and lower sectioned bearing ball support. An AC resistance bridge (Linear Research Inc., LR-700) was used to monitor the electrical resistance between 12.7 mm diameter by 1 mm thick copper disks in a transverse 4 point probe measurement. An electrical connection to the sample was made by stripping the lacquer coat off the middle ~2mm section of a magnet wire then soldering the exposed region to the edge of each disk. Soldered regions were oriented 180° to one another during simulated assembly. The fixture was located in a box convection oven and both the fixture surface and ambient temperature in the oven was monitored using type K thermocouples. The copper substrates were electrically separated from the tooling by glass cover slide interposers possessing vacuum hold down ports.

### ***Assembly Experiments***

Experiment Set 1: The independent variables chosen for this set of experiments were surface finish (rough or smooth), squeeze rate (0.1, 0.5, 1, 5, 10  $\mu\text{m/s}$ ), and ultimate force applied (6 or 12 N). It should be noted that the squeeze rate values stated are nominal due to compliance in the system. At small gap widths, as the resistance to flow and the normal force applied increased, the squeeze rate deviated from this value. The ultimate normal forces reported are also nominal values due to the dependence on the operator to stop the squeeze when the desired force was reached.

To prepare bondline samples, Assembly Approach 1 and Material Deposition Method 1 were applied. The substrates were first attached to the fixturing and zero gap width was observed. After releasing the lower substrate's vacuum hold a nominally conical and 10.3 mg deposit was dispensed near the center of the substrate before it was returned to the fixturing. The assembly sequence was then controlled by the movement of the rheometer. After return of the lower substrate, the movement sequence was: move to a 200  $\mu\text{m}$  gap width from 2 mm at 20  $\mu\text{m/s}$ ; hold for 30 seconds; move at the selected squeeze rate until the selected ultimate normal force was achieved; then hold for 5 minutes at force. After 5 minutes, the vacuum was released, the stage raised, and the sample moved to cure in a convection oven.

Experiment Set 2: Samples were prepared using: Copper Substrate 1; Deposition Method 2; Assembly Approach 2 or 3. Squeeze rates were either 10  $\mu\text{m/s}$  or manually controlled to be  $>10 \mu\text{m/s}$ .

Experiment Set 3: Samples were prepared using: Copper Substrate 2; Deposition Method 1 or 3, Assembly Approach 3 or 4. The independent variables chosen for this set of experiments were squeeze rate (0.75 or 10  $\mu\text{m/s}$ ) and ultimate force (100 or 272 N).

Experiment Set 4: Samples were prepared using: Copper Substrate 2; Deposition Method 1; Assembly Approach 5. The applied compressive load of (30, 150, 300 N) was achieved through setting the air pressure supplied to the pneumatic actuator. The pressure required to achieve the desired load was calibrated using a small form factor load cell placed between the assembly surfaces (Omega, LC302-50).

#### 4. Thermal Characterization

The flash diffusivity method (ASTM E 1461 [9]) was used to measure the back-face temperature vs. time response of trilayer samples to a transient heat pulse. Measurements were performed at room temperature using the Anter Corporation Flashline 2000, a xenon flash bulb-based system. Surfaces were coated with a graphite layer to increase the emissivity of the sample surfaces, which improves coupling to the radiant energy pulse and also provides a uniform back-face target for the optical temperature detector. From this temporal response to the heat pulse, a finite difference numerical model coupled with an optimization code, as provided by Anter Corp., was used to estimate  $R_b$ . This model used inputs of the thermophysical properties of the copper layers in addition to thicknesses values for the substrates to iterate on  $R_b$  and minimize the deviation between the output of the numerical model and the measured temperature response.

#### 5. In Situ Monitoring of Bondline Electrical Performance

Electrical resistance measurements of in situ bondline performance were used to expand our understanding of the bondline formation process. It is well established that for pure metals, such as silver, the majority of heat flow is through electron carriers [10]. The Wiedemann-Franz law describes the relationship between the intrinsic thermal and electrical conductivity of a metal due to electron carrier contribution:

$$T L = \frac{\lambda}{\sigma} \quad (13)$$

where  $T$  = temperature,  $L$  = Lorenz number ( $2.45 \times 10^{-8} \text{ W}/\Omega\text{K}^2$ ),  $\lambda$  = thermal conductivity, and  $\sigma$  = electrical conductivity per [10]. It is useful to modify the above expression into terms of electrical resistance ( $R_e$ ) and  $R_b$ . The definition of  $R_e$  across the bondline being:

$$R_e = \frac{H}{\sigma A_b} \quad (14)$$

and through rearrangement and substitution of Eq.1 and Eq.14 into Eq.13:

$$T L = \frac{\lambda}{\sigma} = \frac{A_b R_e}{R_b} \quad (15)$$

provides such an expression. Note that if the resistance to heat flow rather than flux is substituted for in the above, the  $A_b$  term drops out of the above expression.

For electrically conductive TIMs, it is therefore possible to measure electrical resistance across the bondline as an analog for the thermal resistance of the bondlines during in situ processing studies. This treatment is valid for that portion of heat

transfer due to electron carriers in the electrically continuous filler particle networks extending across  $H$  and ignores the contribution from phonon modes. These phonon carrier contributions can be expected to further increase  $\lambda_b$ .

Using Assembly Approach 5, samples of TIM 2 were prepared with a rapid squeeze rate ( $\dot{h} > 10 \mu\text{m/s}$ ) while monitoring electrical resistance. Limited control over the squeeze rate was possible through air flow rate restriction via needle valves installed in-line from the regulator to the pneumatic actuator. Both the resin component of TIM 1 and the full version of TIM 2 were investigated.

## Results and Discussion

### 1. Polymeric Thermal Interface Material (TIM) Rheology

The flow behavior of TIM 1 in an uncured state was studied using parallel-plate rheology (cf. Fig. 4). The material's resistance to flow was monitored by measuring the torque required to rotate the upper plate at a constant rotation rate vs. the lower stationary plate. This torque value was related to the apparent shear stress developed over the sample in the gap. The rate of rotation was related to the apparent shear rate for the particular gap and plate geometry. The faster the spindle rotated, the higher the shear rate. After ramping through a range of shear rates, the apparent shear stress response data collected was compared with the available constitutive models.

Initially, smooth plates were used to evaluate the material's properties in rotational rheometry. Various gaps were employed; however, the data failed to match the available constitutive models. It was noticed that at high shear rates the effective viscosity data for all gaps were similar while at lower shear rates the effective viscosity depended strongly upon the gap used, an indication of wall-slip behavior. In wall-slip phenomena, a reduced-viscosity particle-depletion layer is present, adjacent to the plate surface. As the gap became smaller, the relative effect of wall-slip became larger.

After changing to roughened plates and conducting the same strain rate sweeps, a power-law trend was observed. By introducing features larger than the thickness of the slip layer the mechanical coupling between sample and rheometer was improved. The rheometer's data analysis suite was then used to conduct parameter estimation.

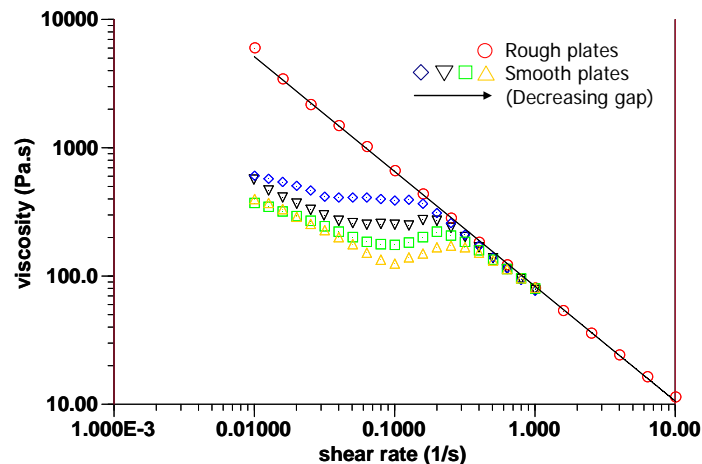


**Fig. 4. Steady rotation rheologic characterization of a silver-flake filled epoxy based TIM, TIM 1. Over the displayed range of shear rates with roughened plates, this material behaved as a power-law fluid (consistency ( $\mathcal{A}$ ):  $83.12 \text{ Pa s}^n$ , rate index ( $n$ ):  $0.105$ ).**

### 2. TIM Bondlines Formed with a Laterally Homogeneous Filler Distribution

#### *Bondline Formation Fluid Dynamics*

During bondline formation for Experiment Set 1 using TIM 1, the temporal normal force ( $F$ ) vs. gap width ( $H$ ) data was collected while the upper substrate was pressed into a single deposit. For relatively large squeeze rates, the material behaved as a homogeneous fluid with a no slip condition at the interfaces. This could then be modeled using a numerical implementation of a standard squeeze flow model for axisymmetric drop spread of a power-law fluid between infinite plates, Eq.9. Using the constitutive equation parameter estimates from the rheological characterization work the behavior observed was largely that of a power-law fluid pressed between parallel plates, Fig. 5.

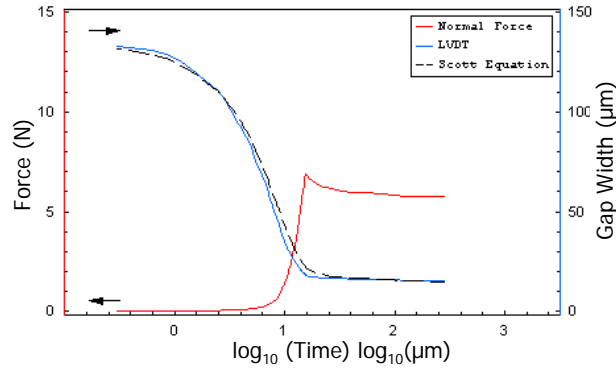


**Fig. 5. Comparison of squeeze data from a 10  $\mu\text{m/s}$  squeeze assembly of a TIM 1 bondline between fully confining smooth glass surfaces to the Scott equation for the axisymmetric squeeze out of a power-law fluid, Eq. 9 [4].**

### ***Thermal Performance of Laterally Homogeneous Bondlines***

Room temperature flash method measurements of the bondline thermal resistance for cured trilayer samples prepared with TIM 2 and a squeeze processes that resulted in a laterally homogeneous filler distribution are presented in Fig. 6. These trilayer samples were part of Experiment Set 2 or 3. The data displayed from Experiment Set 3, indicated by the symbol  $\circ$  in Fig. 6 resulted from samples created with the 10  $\mu\text{m/s}$  squeeze rate. Also included for comparison in Fig. 6 are data measured using silicon substrates in a steady heat flow fluxometer with TIM 2 as prepared using a rapid manual squeeze bondline formation process (similar to Assembly Approach 2 though without Instron motion control) as reported in [11]. The data for samples of bondline thickness less than 20  $\mu\text{m}$  thick were collected from samples cured with a compressive load of 100 N applied.

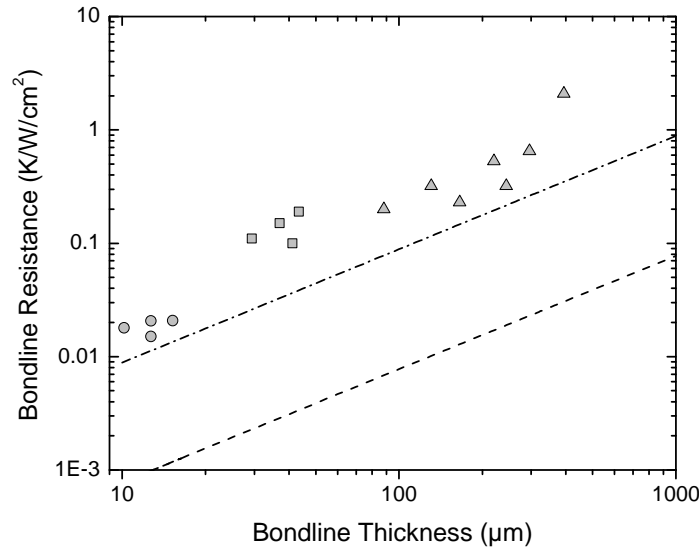


**Fig. 6. Thermal performance of TIM 2 bondlines prepared with relatively fast squeeze assembly rates to ensure a laterally homogeneous filler distribution across the bondline area. Sample data from: Experiment Set 2 ( $\Delta$ ), Steady state fluxometer measurements ( $\square$ ) [11]; Experiment Set 3 ( $\circ$ ). Trend lines show the performance predicted by Eq.1 (---upper line) using the manufacturer supplied  $\lambda_{TIM} = 11.3 \text{ W/mK}$  or the performance predicted by Eq.6 (---lower line)  $\lambda_b = 129 \text{ W/mK}$  for 30% silver fill in an epoxy matrix substituted into Eq.1.**

Samples squeezed with a fast rate exhibited systematically poorer thermal performance than would be predicted with Eq. 1 with the manufacturer data sheet value for TIM 2 thermal conductivity. All three experimental sets shown, including the steady state fluxometer measurements of [11] are consistent with this observation.

### **3. TIM Bondlines Formed with a Laterally Heterogeneous Filler Distribution**

#### ***Onset of Heterogeneity and Evidence of Compaction in Squeeze Flow Data***

For the remainder of the samples from Experiment Set 1, the normal force ( $F$ ) vs. gap width ( $H$ ) data was collected during bondline formation.

A descriptive subset of this data is displayed as Fig. 7. For fast (10  $\mu\text{m/s}$ ) squeeze rate samples, the material behaved as a fluid flowing out between parallel plates and there was little difference between the force vs. gap data between smooth and rough surfaces. The data used to generate Fig. 5. is again displayed in Fig. 7, repeated as the smooth, 10  $\mu\text{m/s}$  case ( $\Delta$ ). Fig. 7 includes data collected after the 12 N compressive force limit was reached. Reduction in the gap width and normal force after this limit was due to continued flow out of material between the substrates that led to a relaxation in the loading column.

Once heterogeneity was prompted in the squeeze-flow bondline formation process, compaction was observed in the force vs. gap diagram of Fig. 7. This was indicated by an increasingly negative slope at small gaps widths for the two slow squeeze cases ( $\blacksquare$  and  $\square$ ) and potentially for the moderate squeeze-rate rough substrate sample shown ( $\bullet$ ). As opposed to particle jamming, where the gap width decrease can cease abruptly resulting in a near vertical force vs. gap trends, compaction occurred over a range of gap widths. This  $F$  vs.  $H$  compaction trend was due to the increase in the effective viscosity of the composite fluid in regions near the stagnant flow zones where matrix material is excluded and the particle filler density increased. Visualization of this increase in particle filler density between substrates of a nominal 1  $\mu\text{m}$  nominal roughness are available in [1].

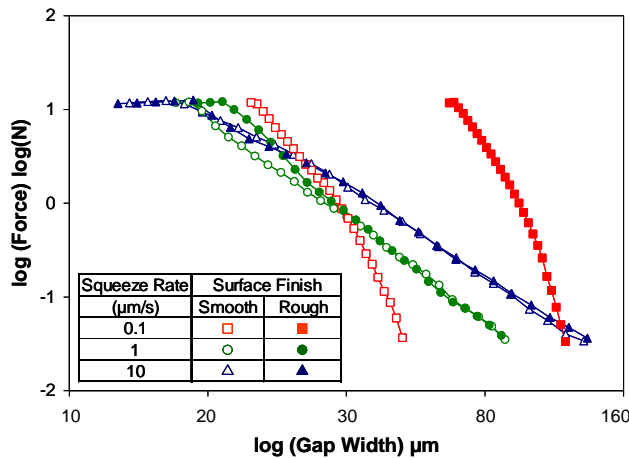


**Fig. 7. Squeeze assembly bondline formation data with TIM 1 using rough or smooth glass substrates (Experiment Set 1) for one of three nominal squeeze rates (0.1, 1, 10  $\mu\text{m/s}$ ). Fast squeezing resulted in behavior as would be expected for a power-law fluid ( $\blacktriangle$  or  $\triangle$ ). Slow squeezing resulted in deviations. Slow squeezing with rough substrates ( $\blacksquare$ ) showed onset of heterogeneity followed by compaction at larger gaps than for smooth substrates ( $\square$ ).**

As predicted by Eq.10, the slower squeeze rate samples exhibited compaction behavior signatures in  $F$  vs.  $H$  data collected during bondline formation. From Fig. 7 it is clear that this onset of flow-induced heterogeneity was greatly impacted by the roughness of the substrate. The rough substrate sample ( $\blacksquare$ ) displayed onset of heterogeneity at a relatively large gap width and resulted in a markedly thicker resultant bondline for an equivalent ultimate normal force as compared to the smooth substrate sample ( $\square$ ). To the author's knowledge, this relationship between substrate roughness and onset of heterogeneity in squeeze flows has yet to be discussed in the scientific literature.

#### **Effect of Compaction on the Thermal Performance of TIM Bondlines**

$R_b$  data for Experiment Set 3 samples were measured using room temperature flash method measurements of cured trilayer samples prepared with TIM 2 between copper substrates, Fig. 8. To increase the likelihood of creating substantial areas of compaction, square substrate samples of Experiment Set 3 had a series of 30 linear rectangular deposits distributed across the entire bondline area prior to bondline formation, thus increasing the number of possible stagnant/compaction regions. The deposit pattern was similar to that shown in Fig. 2e.

From Fig. 8, the three samples prepared with a slow squeeze rate (0.75  $\mu\text{m/s}$ ) performed better thermally than the manufacture  $\lambda_{TIM}$  performance would predict (--- upper trend line of Fig. 8), while the fast squeeze rate sample performed poorer ( $\circ$ ), following the trend for samples of Fig. 6. The slow squeeze sample prepared with a moderate 100 N ( $\Delta$ ) ultimate force resulted in a relatively thick bondline as compared to the other samples of Fig. 8. Following the results displayed in Fig. 7, it appears that the slow squeeze rate prompted flow induced heterogeneity, which developed a compacted filler particle network capable of supporting the applied squeeze force without yielding from the observed bondline thickness. When the squeeze force was increased to 272 N ( $\square$ ) the resultant bondline thickness was observed to decrease, approaching the fast squeeze rate sample's bondline thickness. This decreased bondline thickness indicated that further compaction of the filler network between the substrates had occurred as compared to the moderate force sample.

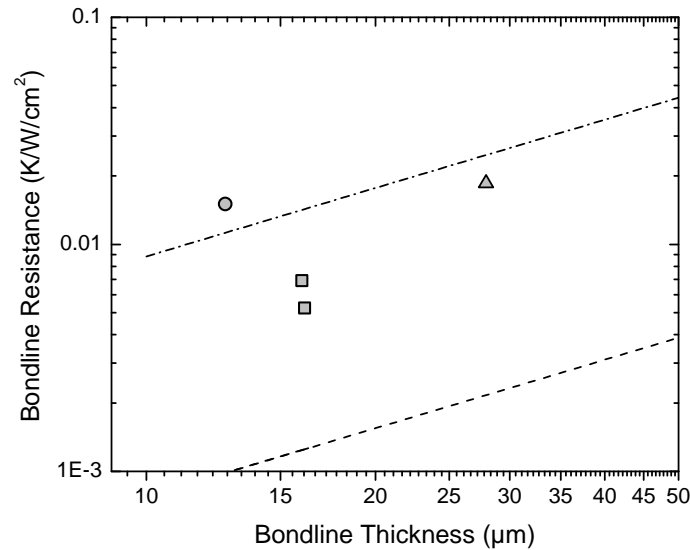


**Fig. 8. Thermal performance of TIM 2 bondlines using a 30 linear rectangular deposit pattern (Material Deposition Method 3). The samples prepared with a slow squeeze rate ( $0.75 \mu\text{m/s}$ ) and large ultimate squeeze force ( $272 \text{ N}$ ) ( $\square$ ) exhibit markedly improved thermal performance over the lower force ( $100 \text{ N}$ ) samples. These being either a fast squeeze rate sample ( $10 \mu\text{m/s}$ ) ( $\circ$ ) or slow squeeze rate sample ( $0.75 \mu\text{m/s}$ ) ( $\Delta$ ). Trend lines show the performance predicted by Eq.1 (---upper line) using the manufacturer supplied  $\lambda_{TIM} = 11.3 \text{ W/mK}$  or the performance predicted by Eq.6 (---lower line)  $\lambda_b = 129 \text{ W/mK}$  for 30% silver fill in an epoxy matrix substituted into Eq.1.**

The thermal data of Fig. 8 demonstrate a marked improvement in bondline thermal performance attributable to a tailored bondline assembly process selected to enhance the creation compacted filler regions in the bondline. The best performing sample was measured to possess a  $R_b$  of  $0.005 \text{ K/W/cm}^2$  and an effective thermal conductivity of  $30 \text{ W/mK}$ . This represents a factor of 4 improvement in the thermal performance over the laterally homogeneous bondline thermal performance and greater than 2.5 factor improvement over the manufacturer  $\lambda_{TIM}$  values. Two process parameters during bondline formation impacted this performance improvement. A slow squeeze rate served to prompt flow induced heterogeneity while a large ultimate compressive squeeze force served to compact the particle network between the substrates.

#### 4. Bondline Stabilization

##### *Effect of System Flexure on Bondline Stability*

In bondline formation prior to any cure operation, the forces applied can result in elastic deformation of the substrate, die, and heat spreader system. Several possibilities exist where such cases of flexure may occur, which would lead to an unstable bondline microstructures after removing the applied load, due to relaxation of the system. For example, it is not unusual for the back side of the die attached to an electronics package to be warped due to expansion mismatches between the board material and silicon die, with the center of the die being taller than the periphery. Should a load applied to the bondline area result in the flattening of the die and substrate, when the load applied through the heat spreader is removed, relaxation of the system would result in one of two scenarios:

1. The TIM displaced towards the periphery from the initial deposit does not provide structural support through the particle network. Such a scenario would drive towards a widening of the gap at the periphery with time after release or the compressive assembly load. This would occur due to the center region existing in a compressive state and the periphery in tension immediately after release of the compressive assembly force.
2. The TIM displaced towards the periphery from the initial deposit provides structural support through the particle network. This is a possibility for solid-filled TIM materials. Such a scenario would drive towards a widening of the gap at the center with time after release or the compressive assembly load. This situation would create a driving force to pull the most mobile species from the periphery to the center of the bondline due to the center region existing in tension and the periphery in compression immediately after release of the compressive assembly force as the system relaxes.

Such a situation, for scenario 2 above, was observed when a silicon die was quickly pressed ( $10 \mu\text{m/s}$ ) into a deposit of TIM 2 where the lower substrate was a transparent glass slide. When the sample was removed from the test fixture and observed through the glass slide substrate air was observed to be drawn in from the periphery. The result is shown in Fig. 9.

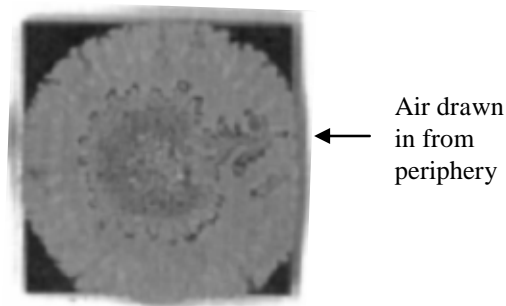


**Fig. 9. Air inclusion due to system flexure after bondline formation and during mechanical relaxation of the assembly after release of load. The sample comprises a 12.7mm double side polished Si substrate square (dark) with TIM 2 applied between it and the transparent glass substrate. Light regions correspond to coverage by the silver-filled TIM. The view is through the glass substrate.**

The example of Fig. 9 is a demonstration of how bondline microstructure and thermal performance may be impacted by insufficient stabilization of the bondline structure after formation. In practice, providing uniform support to the components during bondline formation to minimize system flexure would reduce the degree of such problems. It was found in the study that included the sample from Fig. 9 that increasing the amount of TIM applied reduced the likelihood of air inclusion. However, this would likely not have resulted in a reduction in the driving force to pull the more mobile matrix fluid material to the interior of the sample.

#### ***Effect of Initial Force on Bondline Stability***

One industrial approach to bondline formation is simulated by the experiments displayed in Fig. 10. In this heat-spreader attach process, the TIM is applied to the backside of a die and the heat spreader is placed onto the die deforming the deposit and forming the bondline using the motion of placement machine. After initial bondline formation, the component and lid system is then fitted with a spring or clip before final bondline formation and cure in an oven. The set of experiments in Fig. 10 evaluated the effect of the load applied during the initial bondline formation on the stability of the bondline structure as monitored by the electrical resistance. The stability discussed in this section refers to the stability of the bondline macro and microstructure as evidenced by the electrical resistance once the initial compressive load was released. This resistance was monitored after the initial loading, after a dwell with no applied load, and through the reapplication of a second larger compressive force.

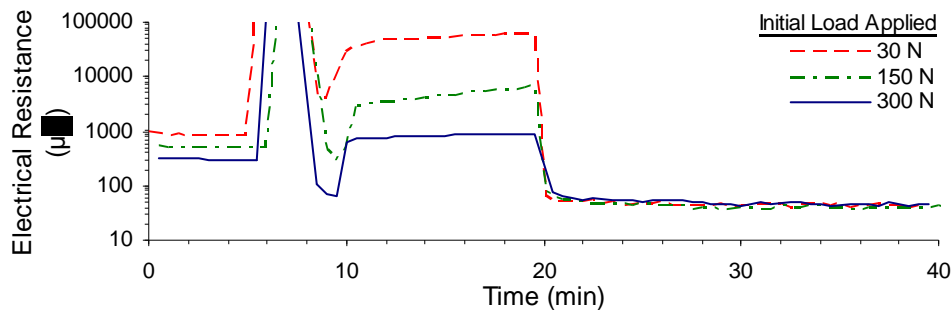


**Fig. 10. Electrical resistance vs. time comparison of 3 in situ experiments varying the initial load applied. Bondlines were formed using TIM 2 between copper coupons. Bare contact resistance between the copper coupons was measured before 5 min. Substrate separation and dispense of a single gap filling deposit onto the lower substrate, Material Deposition Method 1, occurred between 5 and 8.5 minutes. At 8.5 minutes the bondline was formed with the initial load, which was applied for 1.5 minutes. From 10 to 20 minutes the upper piston was completely withdrawn leaving the trilayer sample resting on the lower piston surface. At 20 minutes the upper piston was reapplied using 300 N for 20 minutes. Time scale is shifted to the initiation of the secondary squeeze.**

Two observations can be made from this in situ monitored fast squeeze rate bondline formation experiment. First, the larger the initial force, the more stable the bondline was after the initial load was removed at the completion of the initial bondline formation. As the initial load applied decreased, the rapid increase in electrical resistance upon removal of the initial load increased in magnitude. Second, with the reapplication of a second large force, all samples dropped to the same electrical resistance performance level.

At least for this material and system, any instability that arose after the initial bondline formation and release of the compressive load did not adversely affect the microstructure so much that an observable difference was present in the data. It should be cautioned that as both the upper and lower support structures were surface ground and the samples were flat with parallel faces, this would be a best case scenario. Other assemblies may flex to a greater extent than in this tightly controlled bondline formation process; consequently, these observations may not hold up. Securing the bondline immediately after the initial formation would seem to be a good choice to avoid the uncertainty associated with an additional process sequence prior to final mechanical secure or cure operation.

***Effect of Dwell at Initial Force on Bondline Stability***

Similar to the previous section, the experiments displayed in Fig. 11 were used to simulate the effect of the dwell time during the initial bondline formation on the stability of the bondline structure as monitored by the electrical resistance data. This resistance was monitored after the initial loading, after a dwell with no applied load, and after reapplication of a second larger compressive force.

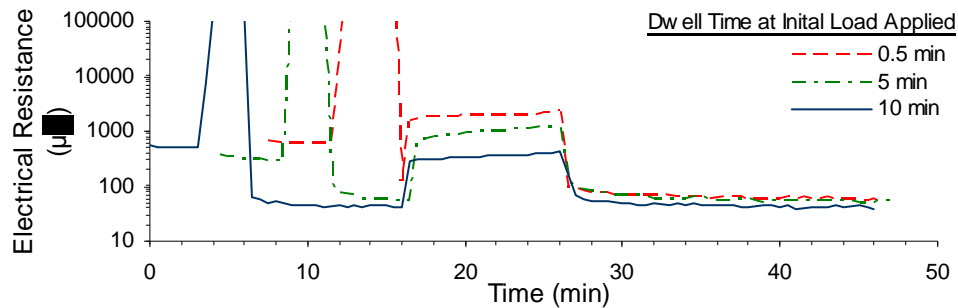


**Fig. 11. Electrical resistance vs. time comparison of 3 in situ experiments varying dwell time during initial bondline formation. Bondlines were formed using TIM 2. Bare contact resistance between the copper coupons is shown in the first 5 min of each data set. The substrates were then separated, material was applied to the lower substrate following Material Deposition Method 1, and the substrates were brought together using 300 N for the selected dwell time. From 16 to 26 minutes the upper piston was completely withdrawn. At 26 minutes the upper piston was reapplied using 300 N for 20 minutes. Time scale is shifted to the initiation of the secondary squeeze.**

These experiments show similar results to those of the experiments displayed in Fig. 10. For a longer dwell time, just as for the case of increased initial force, upon release of the initial bondline formation load the bondline structure was measured to be more stable as compared to the samples prepared with a shorter dwell time, or lighter initial force condition. As the dwell time at initial load applied decreased, the rapid increase in electrical resistance upon removal of the initial load increased in magnitude. After reapplication of the load the electrical resistance again dropped to similarly low levels for all samples. The sample that experienced the longest dwell time during the initial bondline formation resulted in a lower resistance relative to the other samples during the second compressive load application.

***Effect of Stabilizing the Bondline Microstructure on Electrical/Thermal Performance***

The relative electrical resistance performance between a material cross-linked to stabilize the bondline microstructure (---) and a material where the microstructure was not stabilized after formation (—) is shown in Fig. 12. The material with the greater volume fraction of silver fill, TIM 2, exhibited lower thermal resistance values throughout the experiment as compared to the silver-filled epoxy resin of TIM 1. For both samples, after the oven was turned off there was a decrease in the electrical resistance as the sample cooled. Per Eq.13, an analogous drop in the thermal resistance would be expected. When the applied load was removed, the resistance rapidly increased for the silver-filled resin bondline. This was in contrast to the cured TIM 2 bondline, which showed no such increase, indicating that the microstructure had been stabilized by virtue of the metallic fill being locked in place by the cured matrix material.

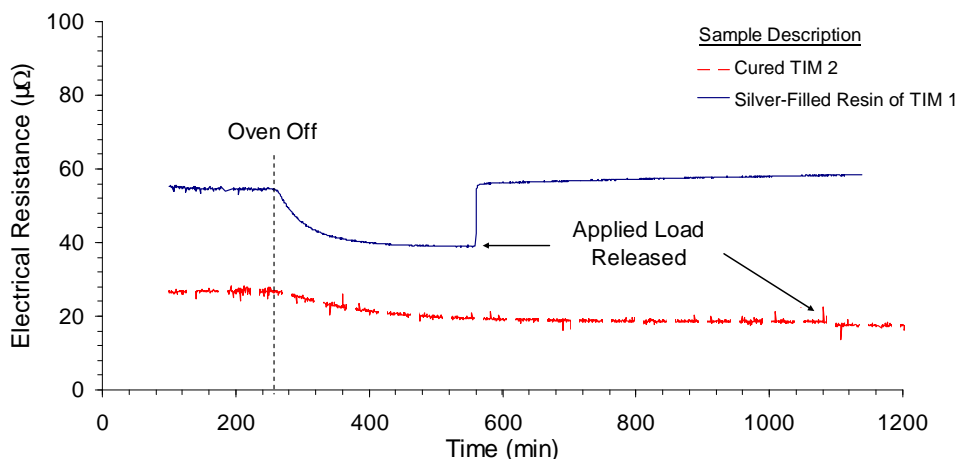


**Fig. 12. Electrical resistance vs. time comparison between an uncured bondline formed with the silver-filled resin component (without hardener) of TIM 1 (—) to the cured sample of TIM 2 (---) after removal of the 300 N compressive load. Time scale is shifted to the shut off of the oven.**

### Conclusion

It was found to be readily possible to create thermal bondlines that, at time zero, have a nominally homogeneous structure. For the curable thermal interface material (TIM) studied, to create this type of bondline through automated bondline assembly the key factors were: 1) taking care in material deposition to avoid entrapment of air at the flow fronts; 2) squeezing the other component into the deposit at a relatively rapid rate during bondline formation; 3) and curing under load using an appropriate temperature profile. The selection of the squeeze rate was dictated by the rheological properties of the TIM and the gap condition. It was demonstrated that, for a material which could be modeled as behaving like a power-law fluid with a no slip layer, this squeeze flow behavior can be reasonably well predicted. When samples were fabricated in such a manner, the resultant thermal behavior was consistently poorer than would be predicted by the manufacturer data sheet. In our experience in testing these materials, this is quite usual.

In complete contradiction to this trend to lower than data sheet performance in bondline configuration, thermal resistance results for an off the shelf silver-filled TIM demonstrated that markedly better than data sheet performance can be attained. This approach is a new avenue to improved bondline performance that does not require investment in new material development or switching from a vetted material system. This increased performance was achieved by: 1) distribution of many initial deposits across the bondline area; 2) varying the squeeze rate at a carefully selected point to include a slow assembly speed to trap particles near the stagnant flow locations; 3) application of a large ultimate force to enhance the extent of compaction of the entrapped particle network; 4) and curing under load using an appropriate temperature profile. While this approach is far from completely optimized and work continues to increase the area of compaction to create more uniformly distributed compaction zones, the current research has demonstrated the ability to dramatically increase the thermal performance of bondlines.

The improvements demonstrated in this work stem from an ongoing study of materials, processing, and resulting properties. In the current study we are systematically working to understand the intrinsic properties of the TIMs including evaluation of rheological model approximations. With this knowledge and in combination with in-situ monitoring of normal forces during assembly it is possible to predict the onset of heterogeneity in order to exploit the compaction observed. With in-situ electrical performance, for the subset of TIMs that rely on electron carriers for heat transport, the electrical resistance was demonstrated to illustrate effects of assembly and heat treatment on the bondline performance. The resulting electrical and thermal characterization work is now being used to guide both new iterations in the processing of materials and to aid in the development of new materials that allow the formulator to balance the tradeoffs between processing ease and lifetime thermal performance and reliability.

### Acknowledgements

This work was part of a major and ongoing research effort supported by the AREA Consortium. In addition, a portion of this work was carried out at Sandia National Laboratories in Albuquerque, NM and at Binghamton University, Binghamton, NY. The support of the Organic Materials Department, Org. 2453 at Sandia National Laboratories and the Research Foundation at Binghamton University is greatly appreciated.

## References

- [1] Rae, D.F., Rightley, M.J., Emerson, J.A., Galloway, J.A., Huber, D.L., Cotts, E.J., and Thermitus, M.A., "Thermal Interface Control: Thermal Performance and Structural Correlations for a Microscale Composite with Dispersed Nanoscale Filler Material," *Thermal Conductivity* 28, R.B. Dinwiddie, M.A. White, and D.L. McElroy, eds., DEStech Publications, pp. 423-434, 2006
- [2] Kittel, C., *Introduction to Solid State Physics*. New York, NY: John Wiley & Sons, Inc., pp. 126, 1995.
- [3] Engmann, J., Servais, C., and Burbidge, A.S., "Squeeze Flow Theory and Applications to Rheometry: A Review," *J. Non-Newtonian Fluid Mech.*, 132:1-27
- [4] Scott, J.R., 1931. "Theory and Application of the Parallel-Plate Plastometer," *Trans. Inst. Rubber Ind.* 7: 169–186
- [5] Laun, H.M., Rady, M., Hassager, O., 1999. "Analytical Solutions for Squeeze Flow with Partial Wall Slip," *J. Non-Newtonian Fluid Mech.*, 81: 1-15
- [6] Delhaye, N., Poitou, A., and Chaouche, M., 2000. "Squeeze Flow of Highly Concentrated Suspensions of Spheres," *J. Non-Newtonian Fluid Mech.*, 94(1): 67-74
- [7] Chaari, F., Racineux, G., Poitou, A., and Chaouche, M., 2003. "Rheological Behavior of Sewage Sludge and Strain-Induced Dewatering," *Rheol. Acta.*, 42(3): 273-279
- [8] Collomb, J., Chaari, F., and Chaouche, M., 2004. "Squeeze Flow of Concentrated Suspensions of Spheres in Newtonian and Shear-Thinning Fluids," *J. Rheology*, 48(2): 405-416
- [9] "ASTM E 1431: Standard Test Method for Thermal Diffusivity of Solids by the Flash Method", *Annual Book of ASTM Standards*, Vol. 15.02, ASTM International, West Conshohocken, PA, 1998
- [10] Kittel, C., *Introduction to Solid State Physics*. New York, NY: John Wiley & Sons, Inc., pp. 166-168, 1995.
- [11] Fullem, T.Z., "Characterization of the Heat Transfer Properties of Thermal Interface Materials," PhD dissertation, Materials Science Program, Binghamton Univ., Binghamton, NY, 2008



# Optimizing the Automated Assembly Process for Filled Polymer Based Thermal Bondlines

David F. Rae<sup>1,2</sup>, Peter Borgesen<sup>1,2</sup>, and Eric J. Cotts<sup>2</sup>

IPC APEX Expo, Las Vegas, Nevada

Wednesday, April 1<sup>st</sup>, 2008

<sup>1</sup> Unovis Solutions  
Binghamton, NY 13904



*Advanced Process Laboratory*  
*A Division of Universal Instruments Corp*

<sup>2</sup> Binghamton University  
Binghamton, NY 13902

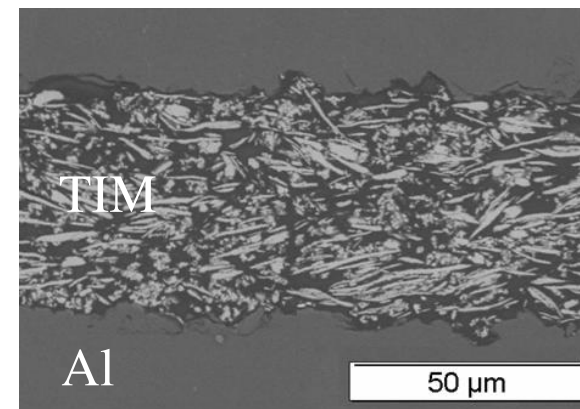
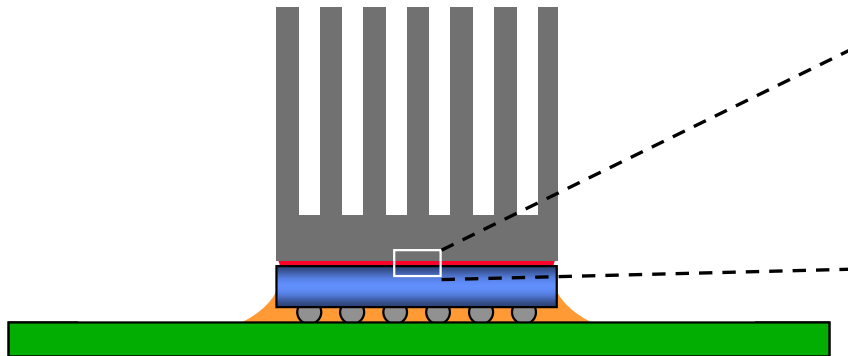


*State University of New York*

## Project Background

In-situ, thermal interface materials rarely (if ever) match the thermal performance displayed on their data sheets. **However, we have been able to demonstrate an average thermal resistance much *better* than predicted by the data sheet.**

As device heat flux values increase, assemblers must minimize the thermal resistance of their interface regions. Defects such as voids, heterogeneity, and unnecessarily thick bondlines can be introduced during the assembly operations. In their product life, material degradation, delamination, and mechanical pump out can occur. These defects generally reduce lifetime thermal performance.





## Project Objectives

- Understand the effects of processing on bondline structure and thermal performance
  - Material deposition
  - Bondline formation
  - Cure or post formation heat treatment
- Develop generalized recommendations for how to produce high performance thermal bondlines
- Provide methods for how to benchmark new materials
- Identify promising new or near to market products
- Generate lifetime reliability data for these material sets



# Presentation Flow

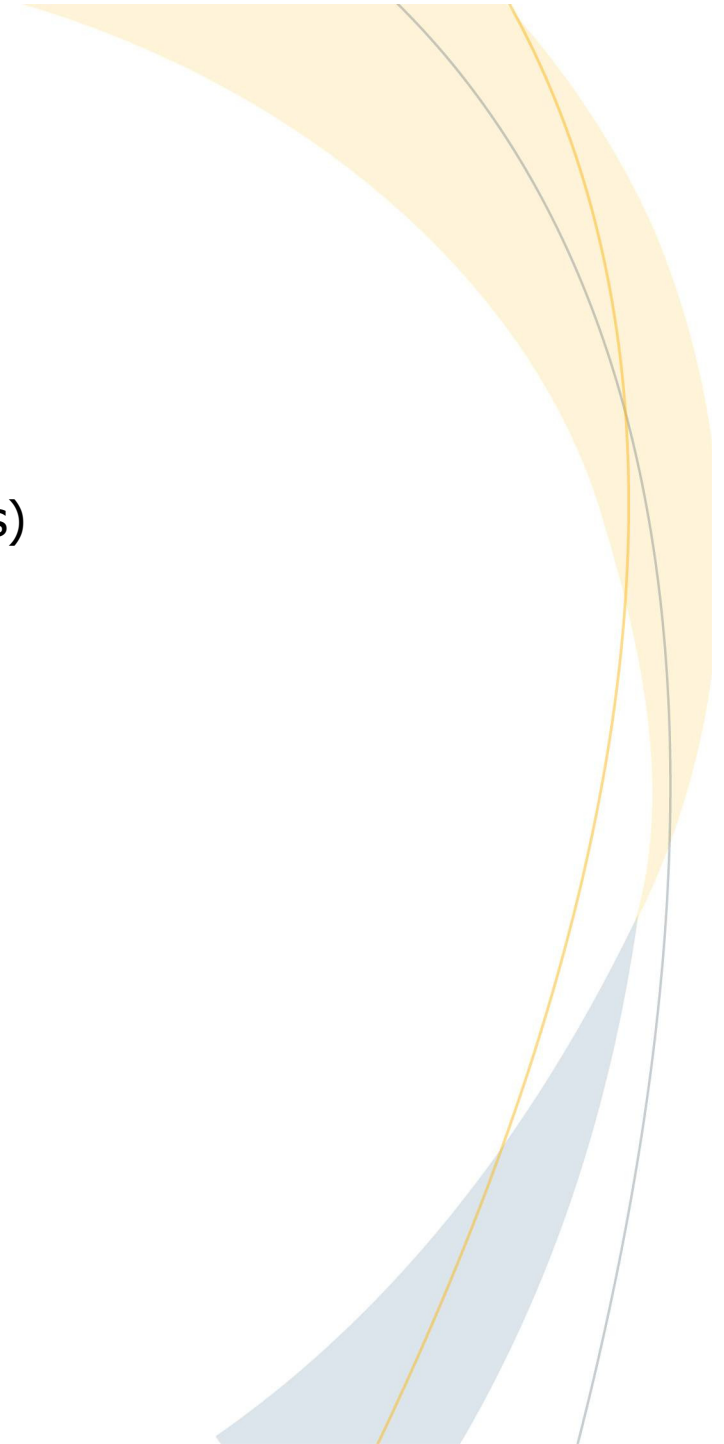
Overview

Approach

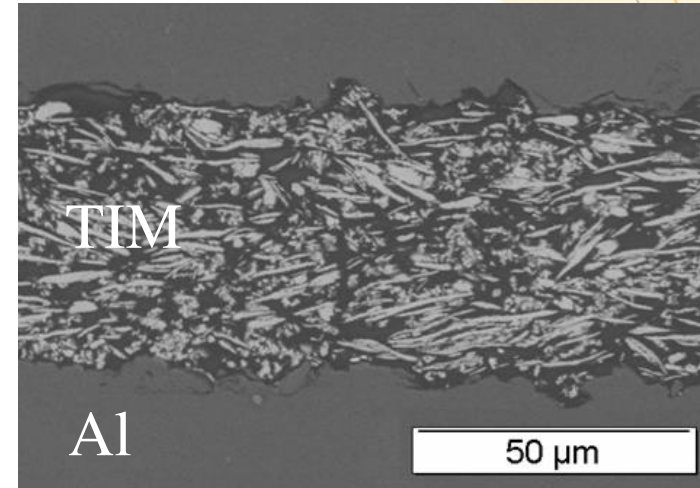
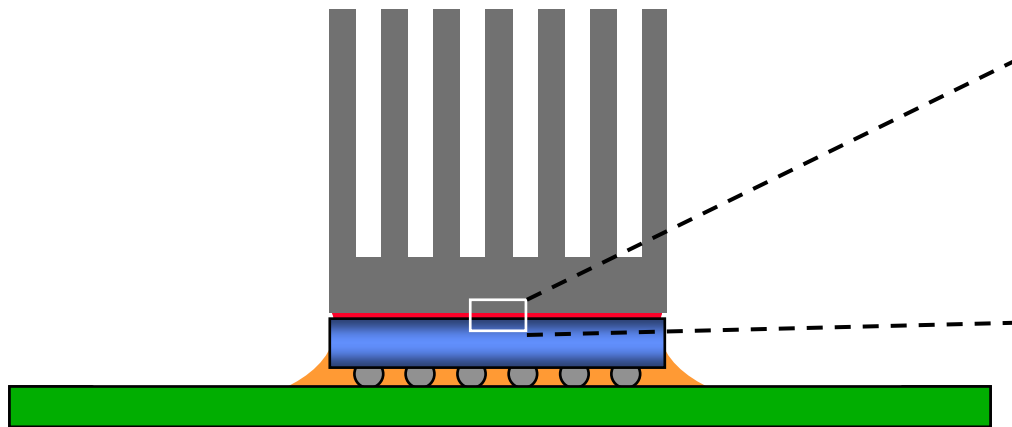
Results

- Benchmarking thermal interface materials (TIMs)
- Stabilization of the bondline post formation
- Optimizing bondline thermal performance

Summary



# Minimize Thermal Bondline Resistance



$$R_{\text{bondline}} = \frac{\Delta T_{\text{bondline}}}{q} = \frac{BLT}{\lambda_{\text{TIM}}} + 2R_{\text{contact}}$$

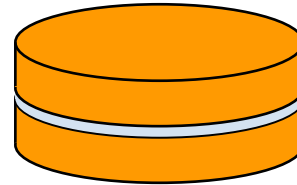
## Thermal Bondline Resistance:

- Decreases with the TIM's in situ effective thermal conductivity ( $\lambda_{\text{TIM}}$ )
- Increases with bondline thickness (BLT) and contact resistance ( $R_{\text{contact}}$ ) that can be attributed to scattering at interfaces and defects near the interface such as voids and particle depletion
- Will be the thermal performance metric discussed

# Sample Description and Thermal Resistance Measurement

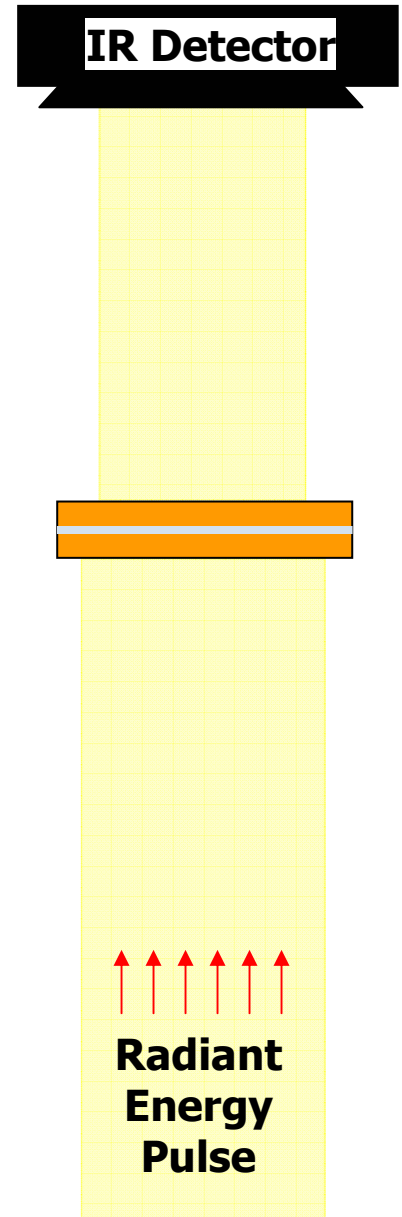
## Bondline samples

- Copper substrates
- 12.7 mm or 11 mm disks or squares
- 1 mm thick
- Generally #8 near mirror finish
- Rough surfaces produced via etch or abrasive paper

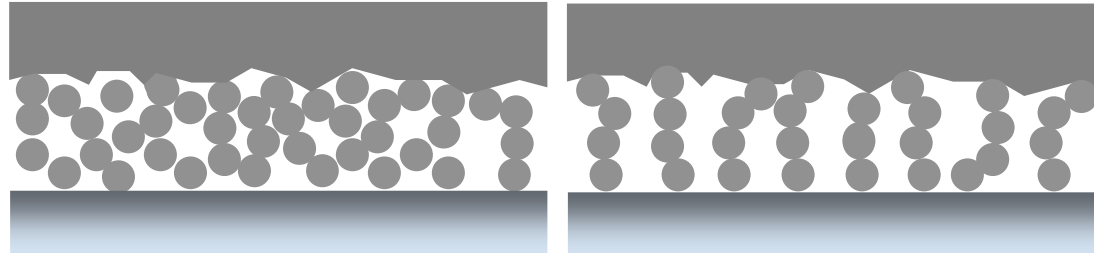


## Flash diffusivity tool (*Anter Flashline 2000*)

- Transient heat pulse incident on bottom face
- Temperature rise measured at top face
- Output
  - Bulk thermal diffusivity of samples
  - Bondline thermal resistance



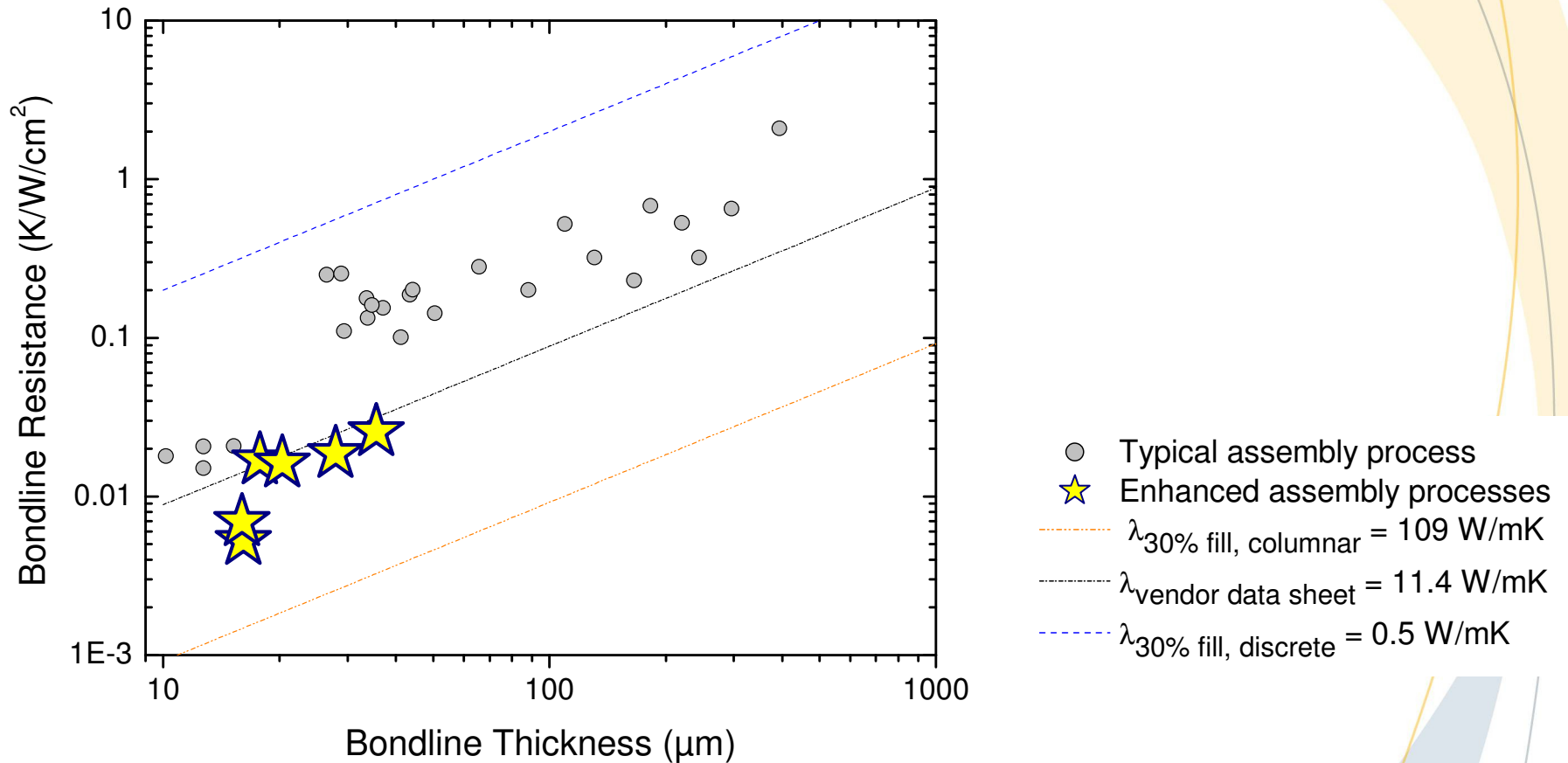
## Bondline Thermal Performance Depends on Microstructure



1. Typical bondline microstructure

2. Best case:  
resistors in parallel;  
particles in contact or  
near contact

# Effect of Tailored Heterogeneity on Thermal Performance



- A 3 X improvement in thermal performance realized for a commercial TIM



# Presentation Flow

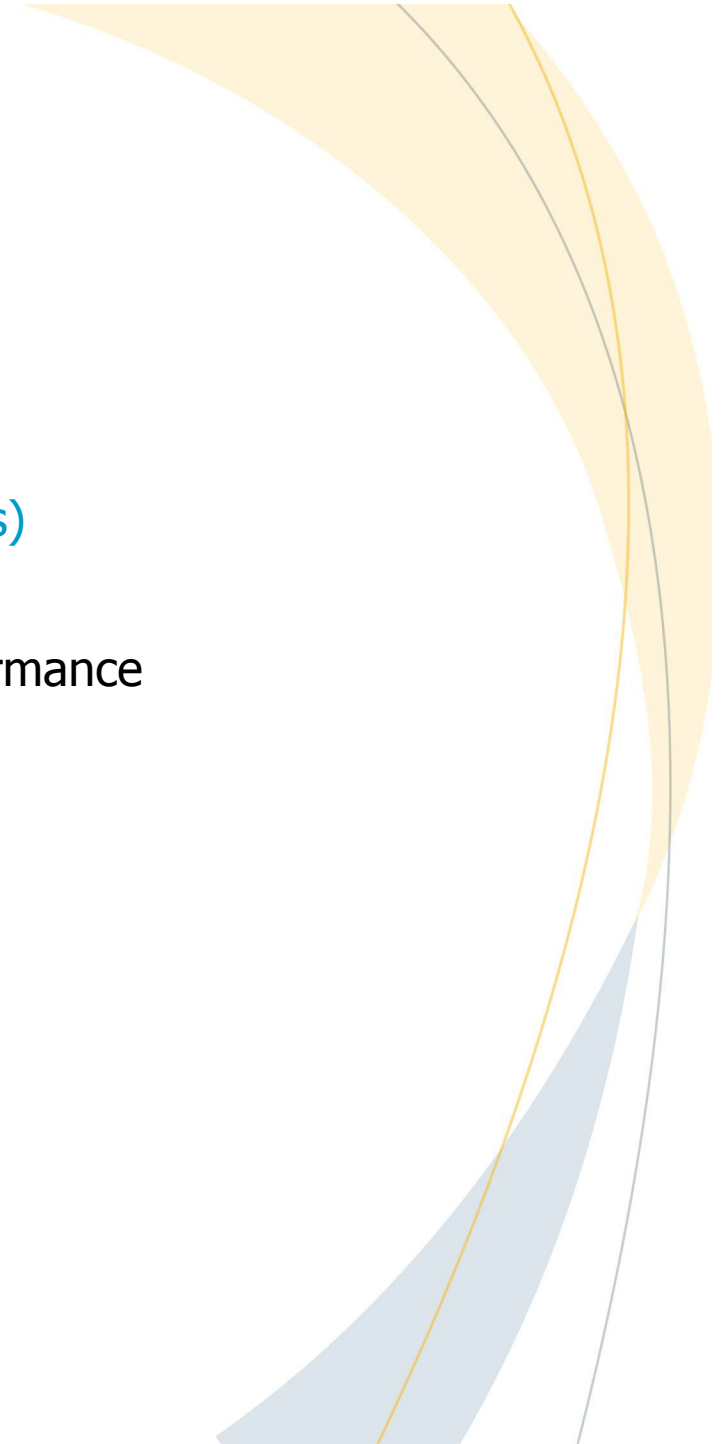
Overview

Approach

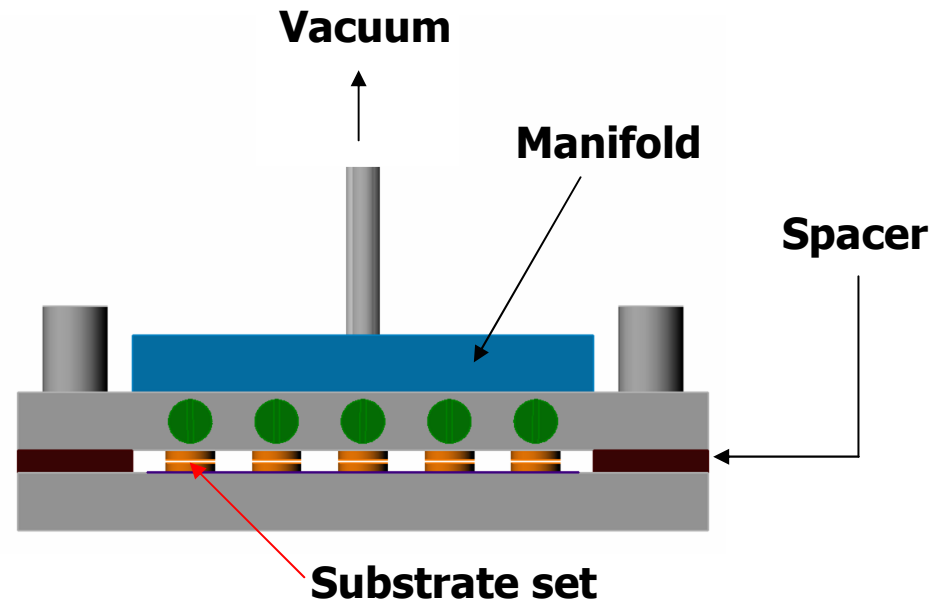
Results

- Benchmarking thermal interface materials (TIMs)
- Importance of stabilizing the bondline structure
- Enhancing bondline assembly for thermal performance

Summary



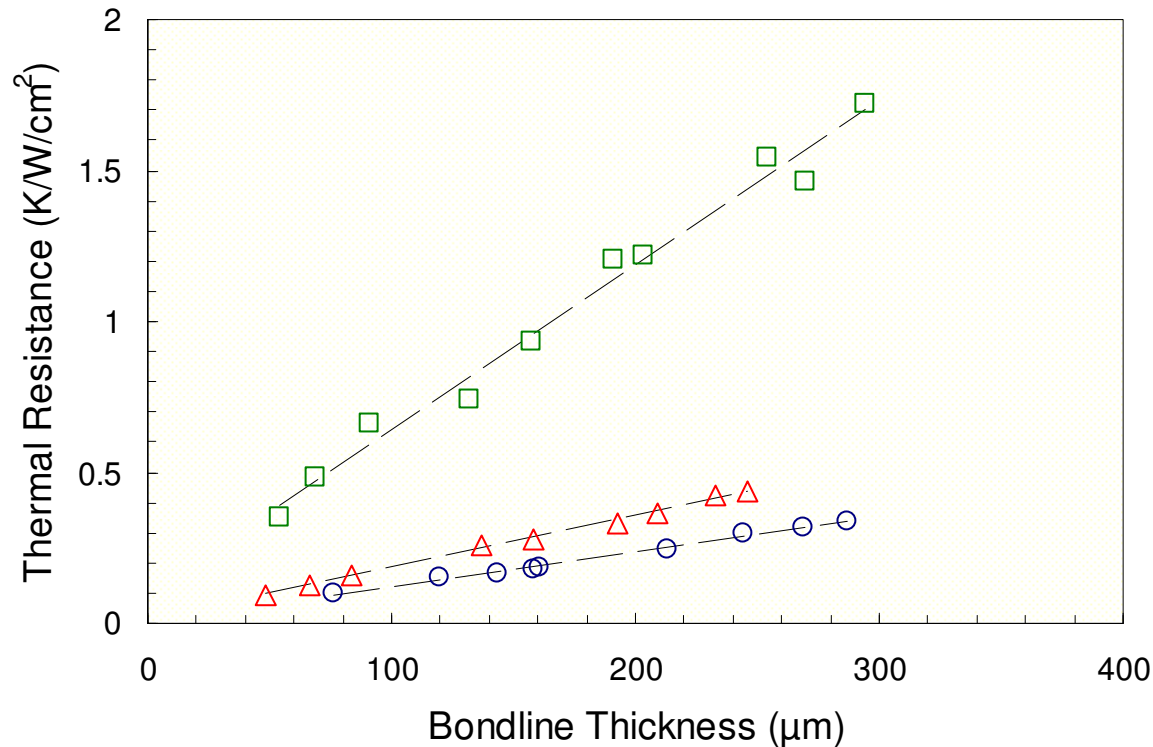
## Thermal Benchmarking TIMs: Multi-Sample Bondline Press



### Features

- Material is dispensed on lower substrate, upper is held in place by vacuum
- Top support features 5 surface ground steps that increment the gap by 20  $\mu\text{m}$
- Surface ground spacers set the gap between upper and lower support
- Spacer sets are incremented by 100  $\mu\text{m}$  which allows a bondline thickness range of 200  $\mu\text{m}$  over the 10 samples when both presses are used
- Located in nitrogen box oven during elevated temperature cure

# Thermal Benchmarking TIMs: Thermal Results



$$R_{\text{bondline}} = \frac{BLT}{\lambda_{\text{TIM}}} + 2R_{\text{contact}}$$

Three TIMs fabricated in multi-sample press and characterized via flash method

- Apparent thermal conductivity calculated from 1/slope
- Contact resistance is 1/2 the value of the intercept
- Approach avoids variation inherent in making samples one at a time
- Allows benchmarking of materials and automated assembly processes



# Presentation Flow

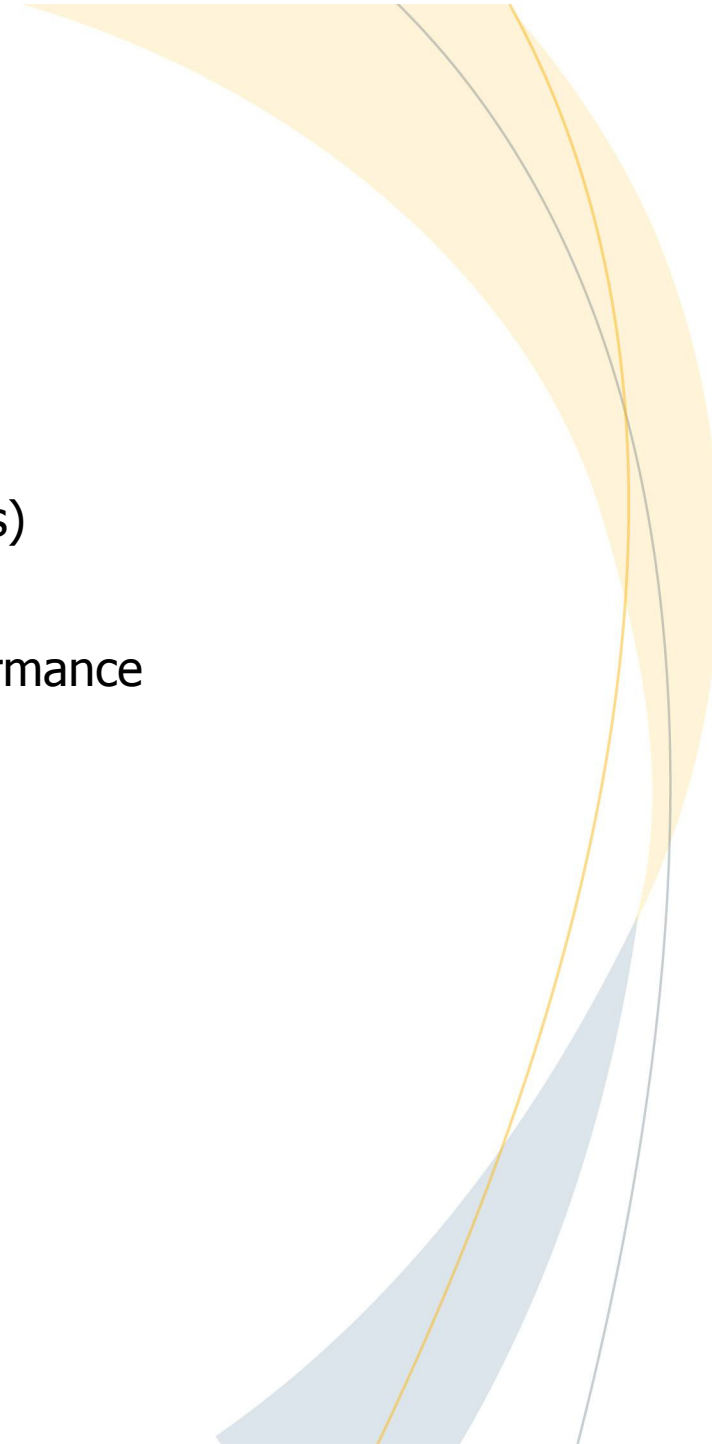
Overview

Approach

Results

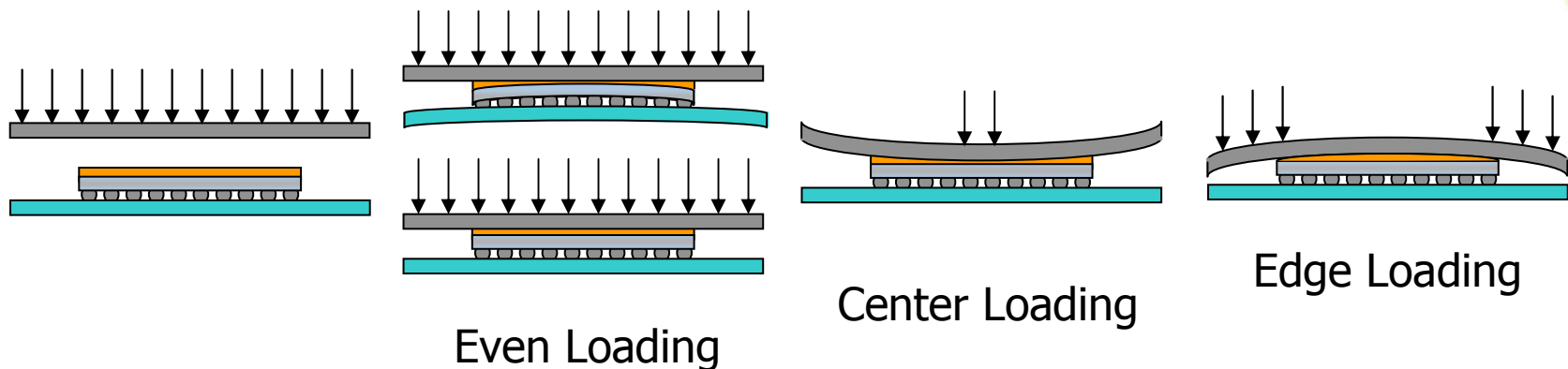
- Benchmarking thermal interface materials (TIMs)
- Importance of stabilizing the bondline structure
- Enhancing bondline assembly for thermal performance

Summary



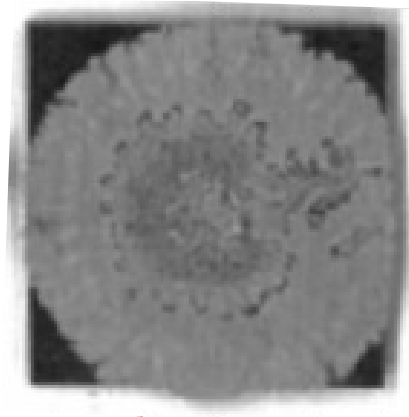
## Effect of Flexure on Bondline Stability

Application of an uneven loading force during bondline formation may detrimentally effect bondline microstructure and performance.



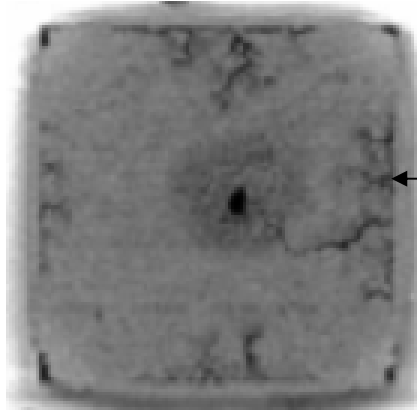
- Even loading, rigid lid & flat die = stable bondline when load is removed
- Center loading that elastically deforms the substrate and die or lid to create a relatively thin region at the center during loading = tension at the center and compression at the edges when the load is removed
- Edge loading that elastically deforms the substrate and die or lid to create relatively thin regions at the periphery during loading = compression at the center and tension at the edges when the load is removed

## Effect of Flexure on Bondline Structure – Center Load Example



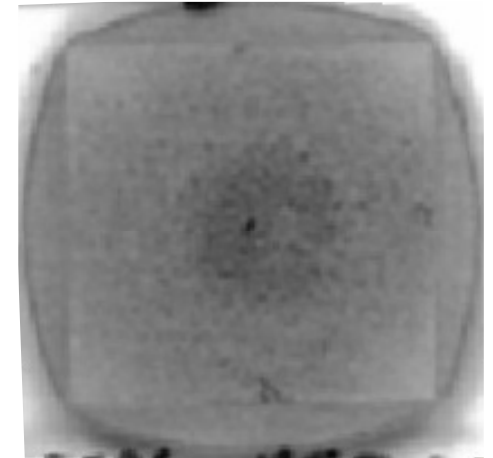
Air drawn  
in here

Insufficient material



Air/Matrix  
material  
drawn in

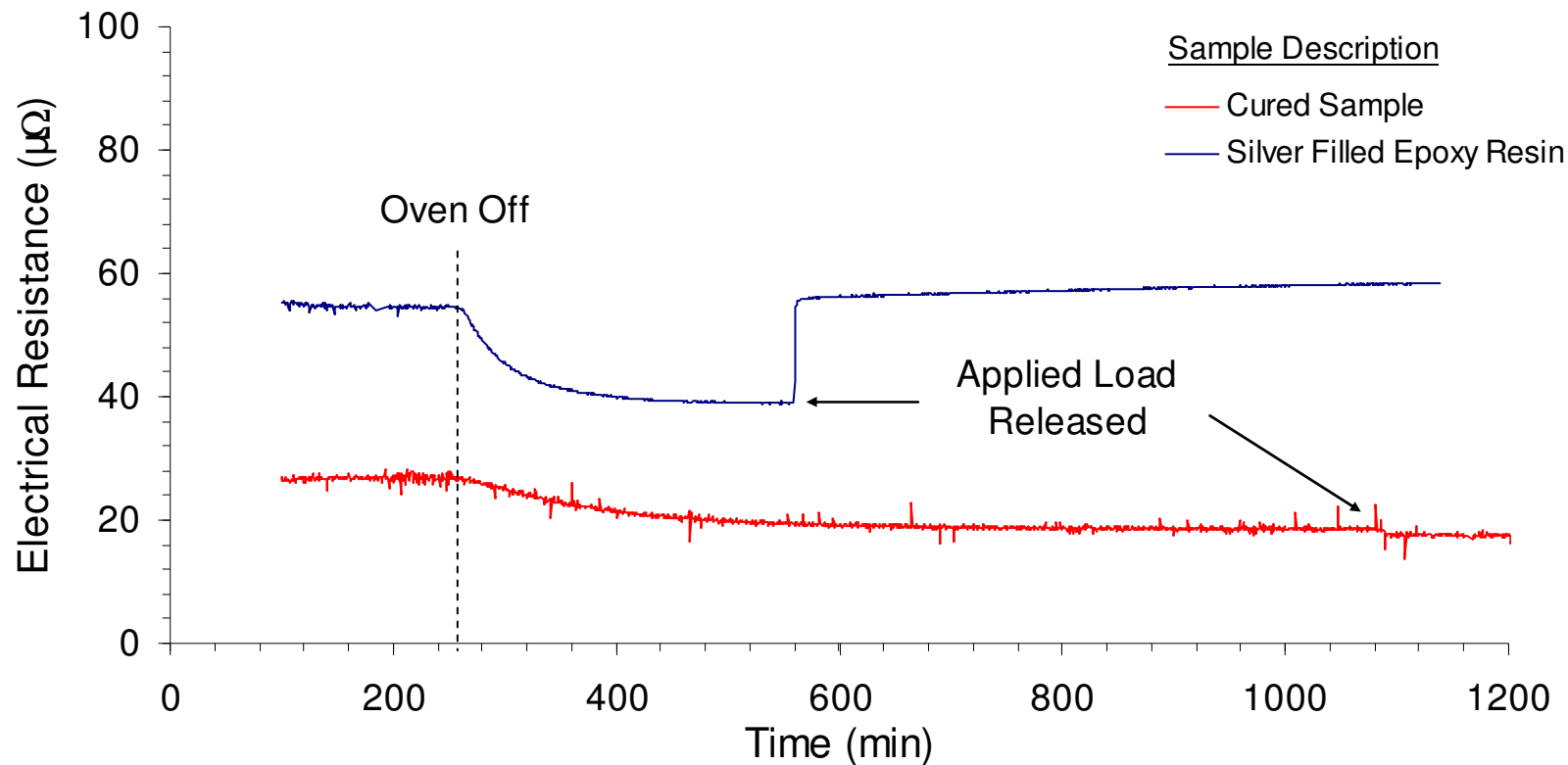
Full Coverage



Excess material

- Silicon shows dark here, silver particles as light, black dot at center is ink
- Significant air suck ingress observed for sample with insufficient material applied
- Excess material eliminated air intrusion however, the driving force still exists implying instability

## In Situ Evaluation of Bondline Formation – Effect of Cure Under Load



- 300 N was applied throughout temperature excursion to 150°C and after the oven was turned off
- For both samples, when the oven was turned off and the samples cooled electrical resistance improved
- The silver filled resin increased in resistance after the piston was removed while the cured sample remained at the same low resistance



# Presentation Flow

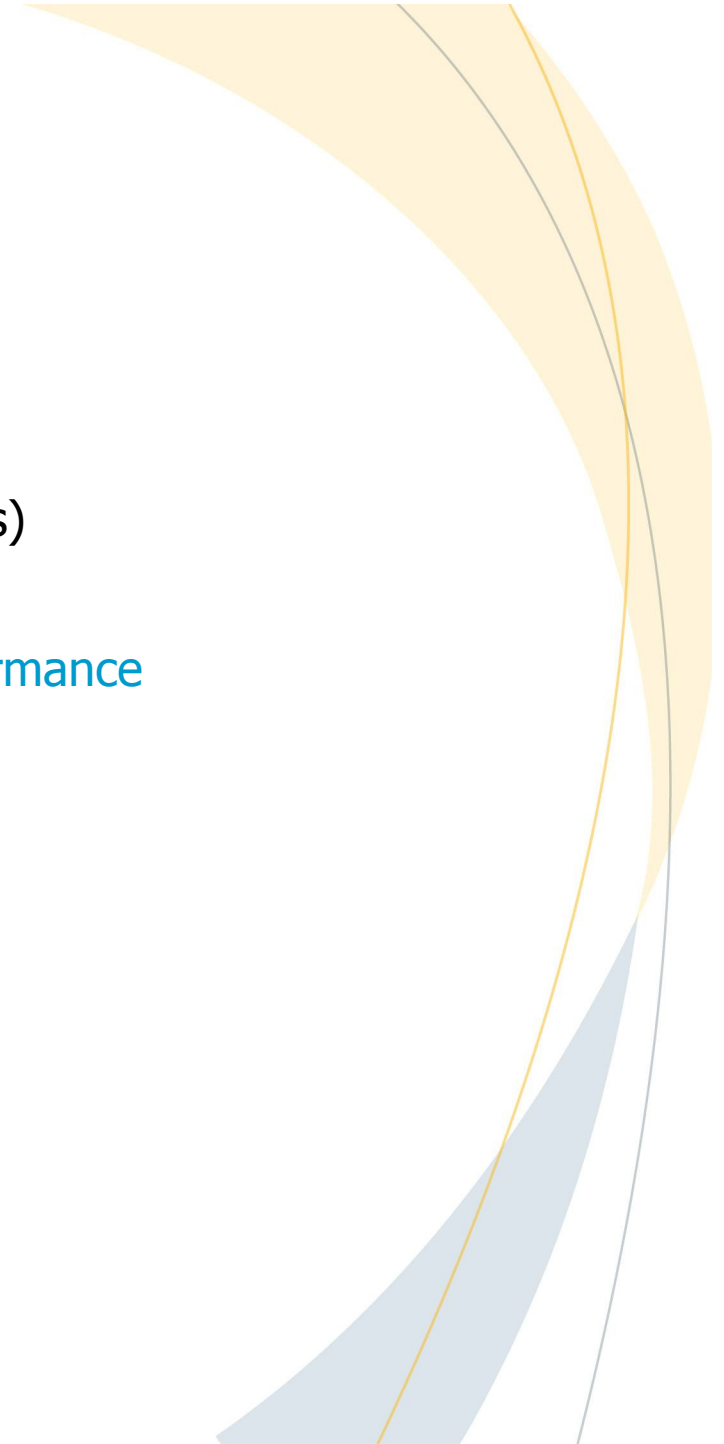
Overview

Approach

Results

- Benchmarking thermal interface materials (TIMs)
- Importance of stabilizing the bondline structure
- Enhancing bondline assembly for thermal performance

Summary



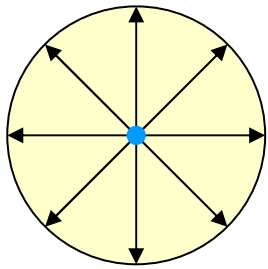


## Two Approaches for Optimization

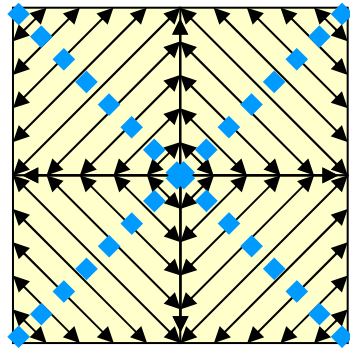
Compacted filler regions are thermally beneficial, acting as resistors in parallel. The key is to distributed them at a small scale across the bondline area.

- 1) Deposition: Optimize pattern to initiate compaction at numerous locations.
- 2) Processing:
  - A. Optimize squeeze flow bondline formation parameters to ensure compaction
  - B. Vibration/scrubbing/oscillation at the end of bondline formation
  - C. Optimize cure parameters (temperature profile and applied compressive load)

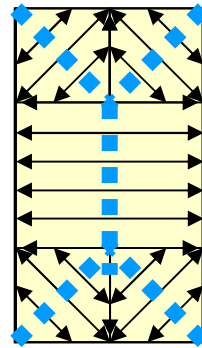
# Optimize Deposition Pattern



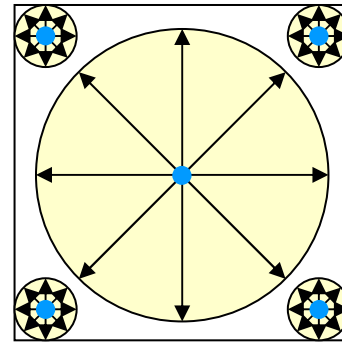
Disk



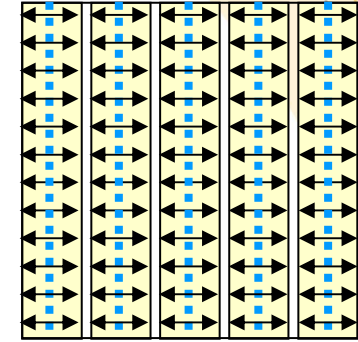
Square



Rectangle



5 dot



Series of lines

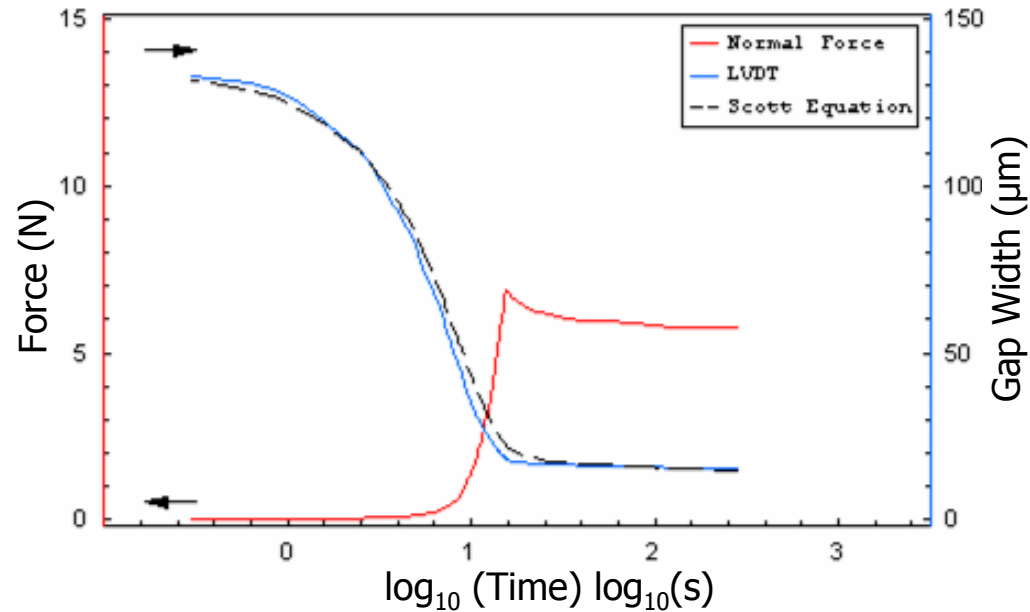
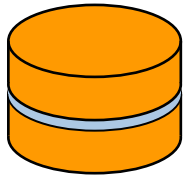
Full Coverage of Gap with TIM

Partial Coverage

- Stagnant regions (shown in blue) occur where the shear rates are zero (these patterns assume uniform loading across bondline area and are approximate)
- Near these locations the flow can be slow enough that it may be insufficient to move particles with the carrier fluid
- Patterns can be used to enhance or minimize heterogeneity in the structure
- Stagnant length of a pattern of 30 lines is 10X that of the diagonals of the fully filled square



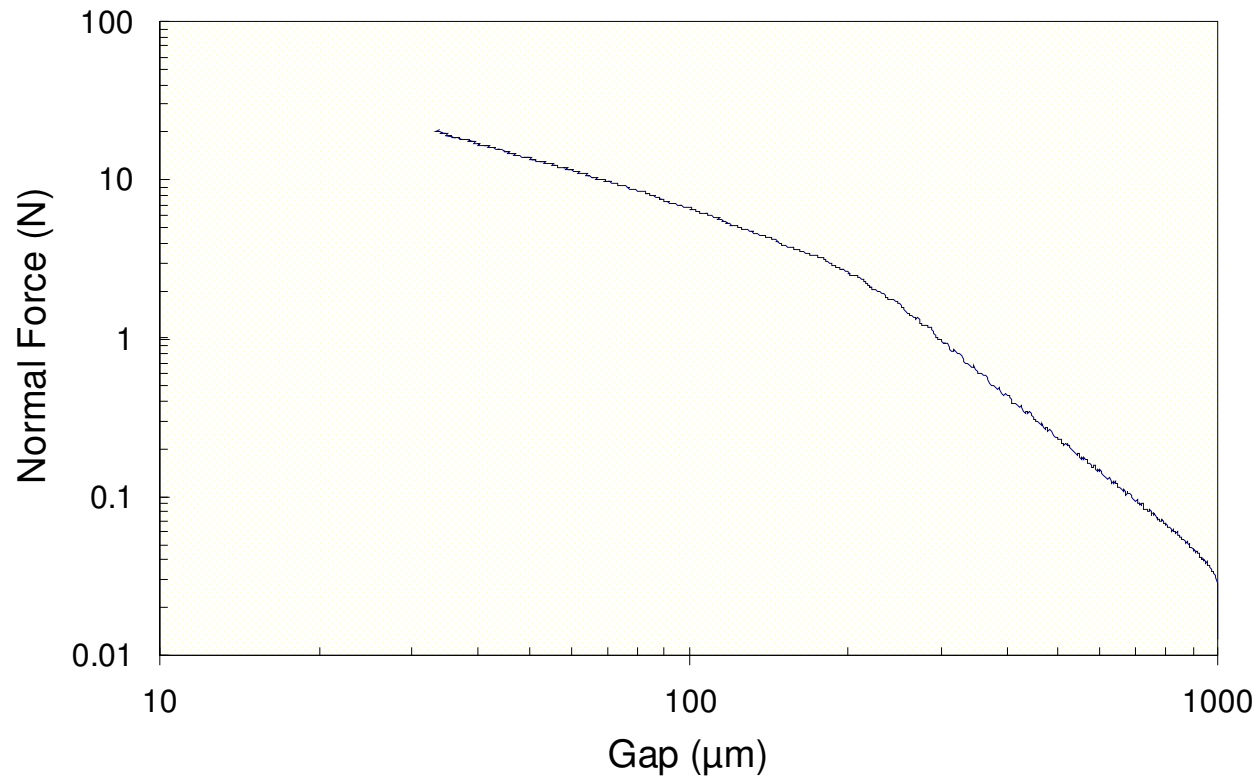
# Squeeze Flow Process Optimization



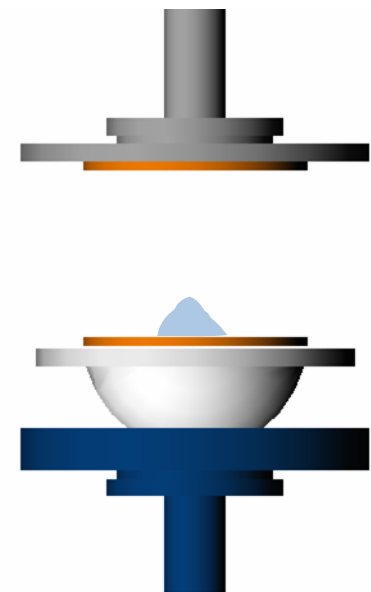
$$F_{\text{shear contribution}} = \frac{-\dot{h}^n}{H^{2n+1}} \left( \frac{2n+1}{2n} \right)^n \frac{\pi k R^{n+3}}{n+3} (1-2\delta)^n$$

- In situ monitoring of bondline formation via temporal normal force and gap measurement in a rheometer (*TA Instruments ARES*)
- Laun model [Laun, 1999] works well for homogeneous power law flows
- Reduces to Scott equation [Scott, 1935] for no-slip boundary condition  $\delta = 0$

# Monitoring Bondline Formation

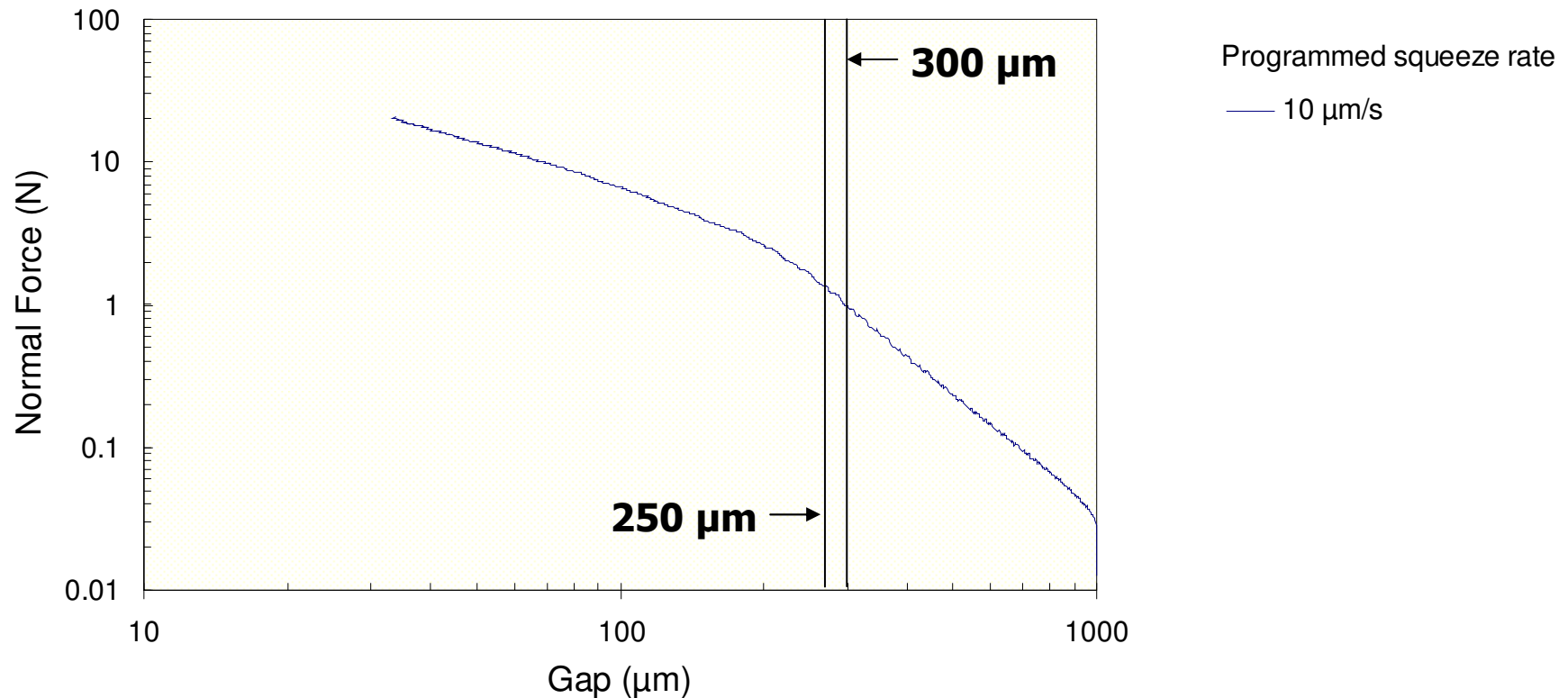


Programmed squeeze rate  
— 10 μm/s



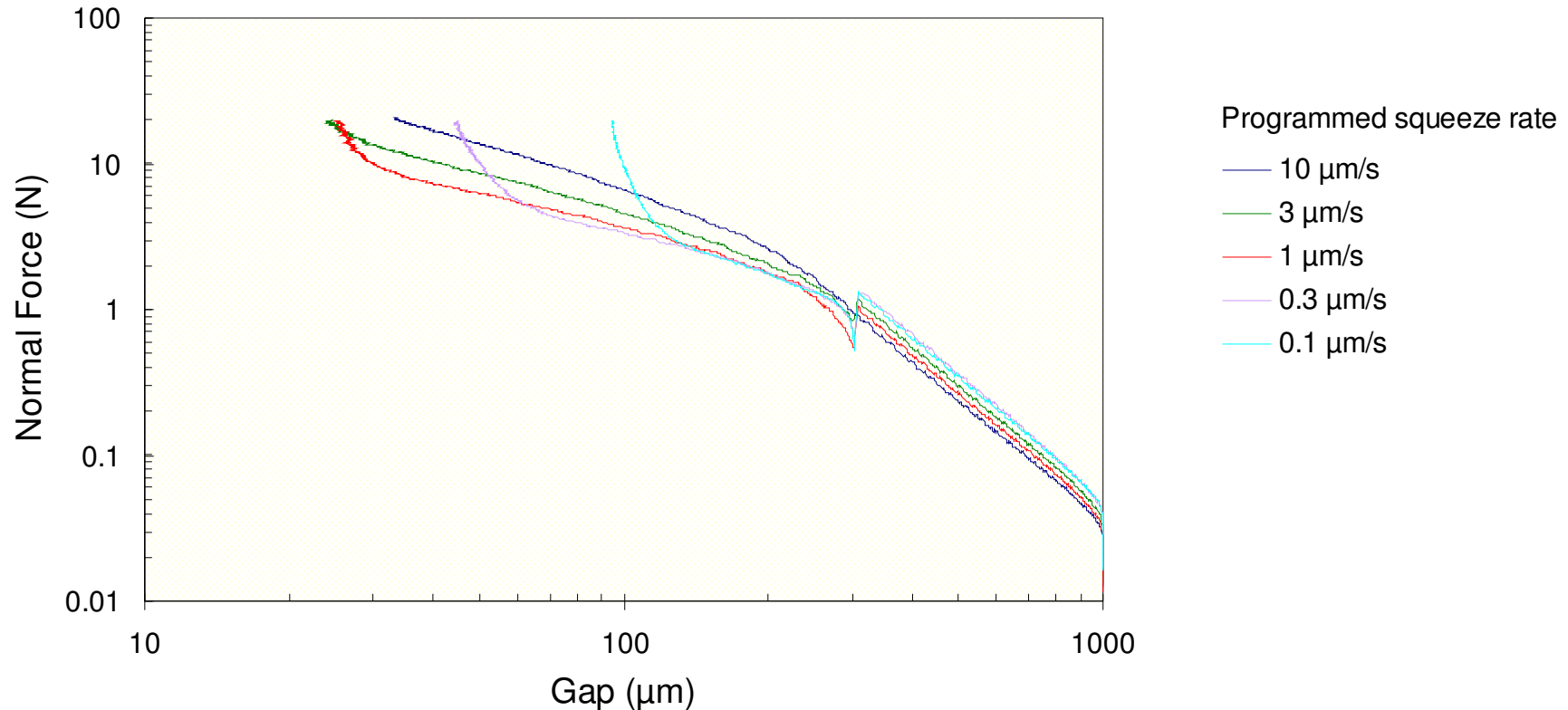
- Force vs. gap diagram allow a study of the effects of varying process parameters on bondline formation

# Monitoring Bondline Formation



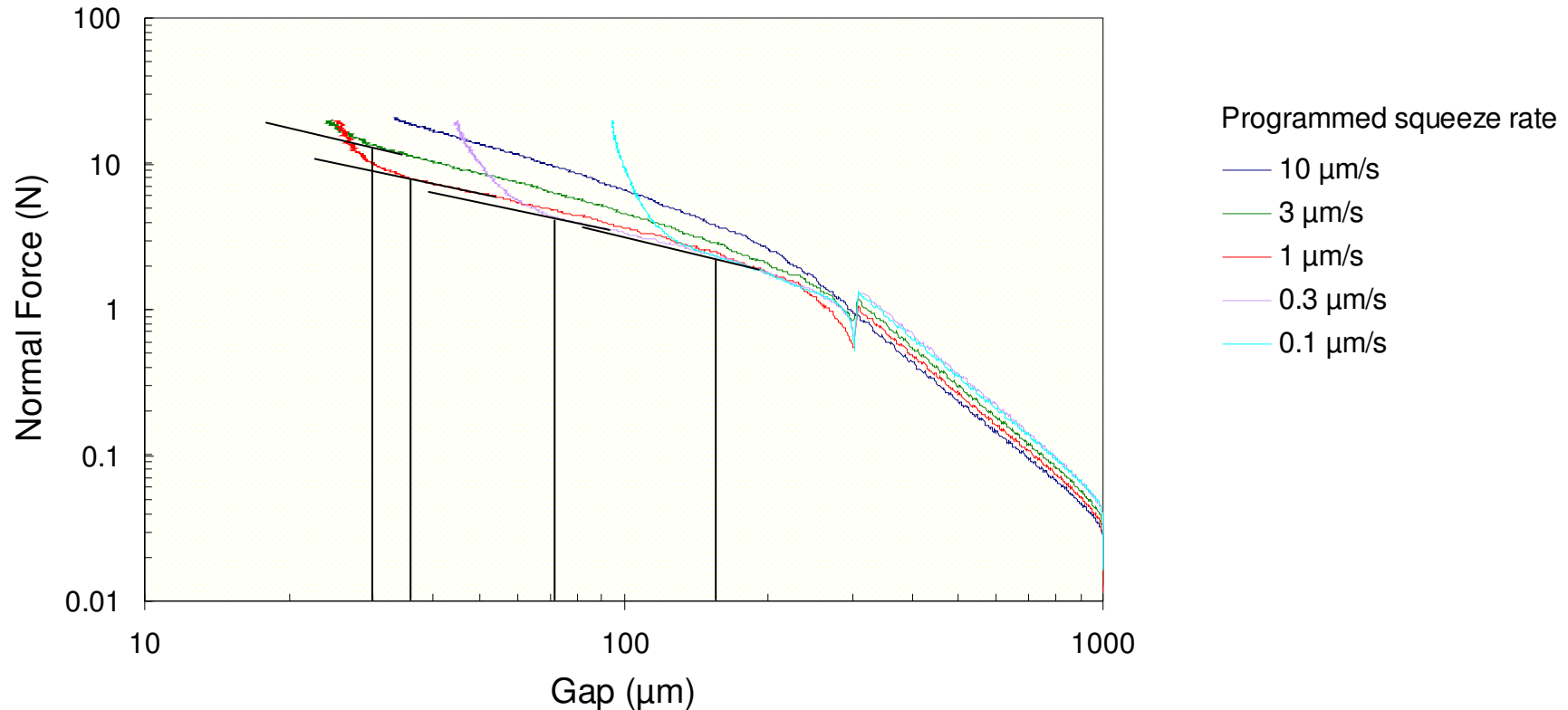
- Samples squeezed at 10  $\mu\text{m/s}$  until a 300  $\mu\text{m}$  gap width reached
- At 300  $\mu\text{m}$ , the programmed squeeze rate was applied
- At 250  $\mu\text{m}$ , the gap between the substrates was fully filled with material
- As force increased the squeeze rate slowed and there was deviation from linear trend towards lower forces
- Experiment halted at load cell capacity of 20 N

## Effect of Squeeze Rate



- At large gaps, the scatter is due to the variation in the amount dispensed onto the lower substrate (more material = larger force)
- Deviation towards large forces for a particular gap indicates the start of the particle dominated stage of bondline formation

## Effect of Squeeze Rate



- Note the gap at which the force deviates; we define this as the onset of heterogeneity
- From onset to final gap, filler matrix fluid is excluded around low shear zones
- The wider this compaction range, the greater the induced heterogeneity

Peclet number:

$$Pe = \frac{\tau_w}{\tau_s} \quad [\text{Collomb et al., 2004}]$$

Where:

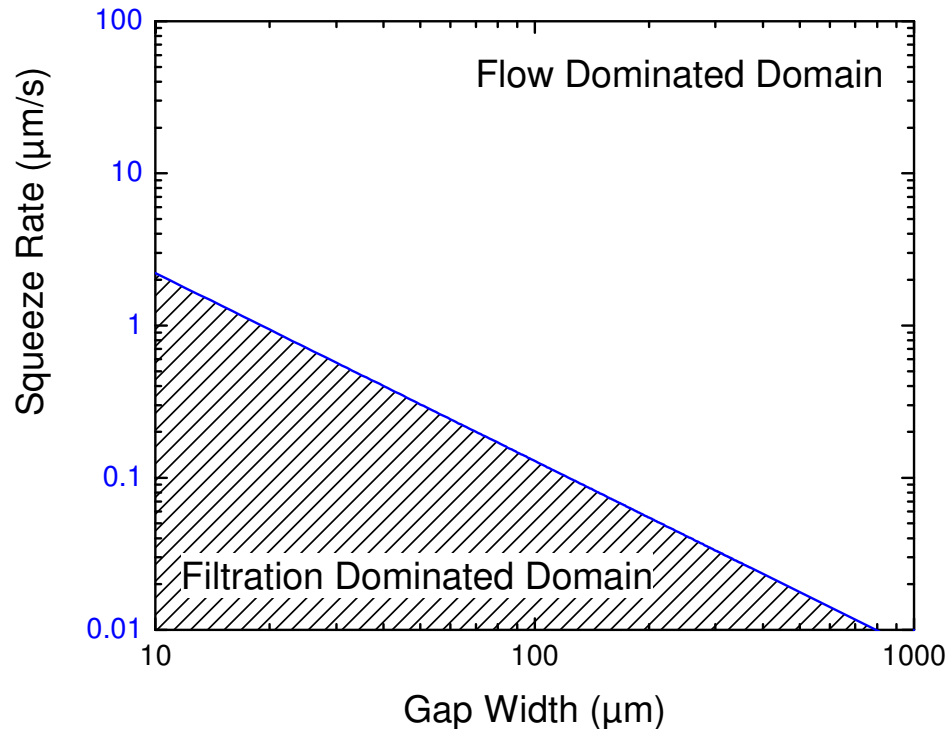
- $\tau_w$  - characteristic time for fluid filtration through a porous media
- $\tau_s$  - characteristic time for deformation of the composite
- $Pe < 1$  corresponds to compaction

$$Pe = \frac{\mu_w \dot{h}_c^{1-m} H^{m+1}}{Ak} \quad \dot{h}_c = \left( \frac{Ak}{\mu_w H^{m+1}} \right)^{1/1-m}$$

And:

- $\dot{h}_c$  - critical squeeze rate below which, for a given gap (H) compaction is predicted
- Note: process parameter values discussed in this presentation are material dependent, behaviors are scalable

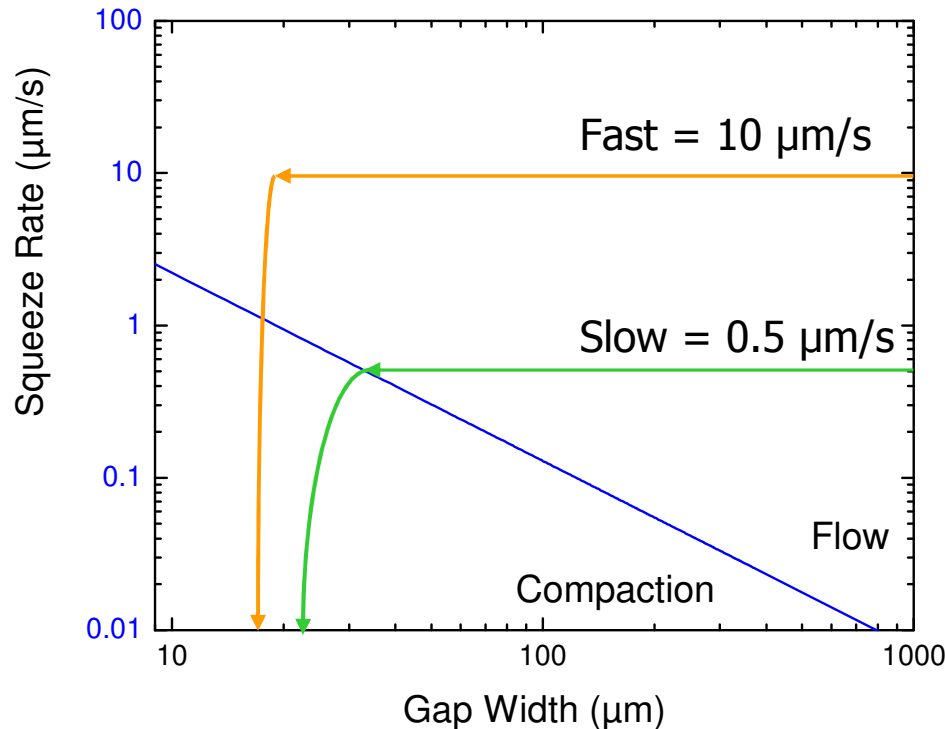
# Exploiting Compaction - Displacement Control



$$\dot{h}_c = \left( \frac{Ak}{\mu_w H^{m+1}} \right)^{1/1-m}$$

- Bondline thickness (gap width) decreases during processing until the point that the filler particle network supports the load applied
  - For a rapid squeeze, this occurs at several effective particle diameters
  - For a slow squeeze crossing into the filtration zone, this occurs after compaction of the filler network near the stagnation zones

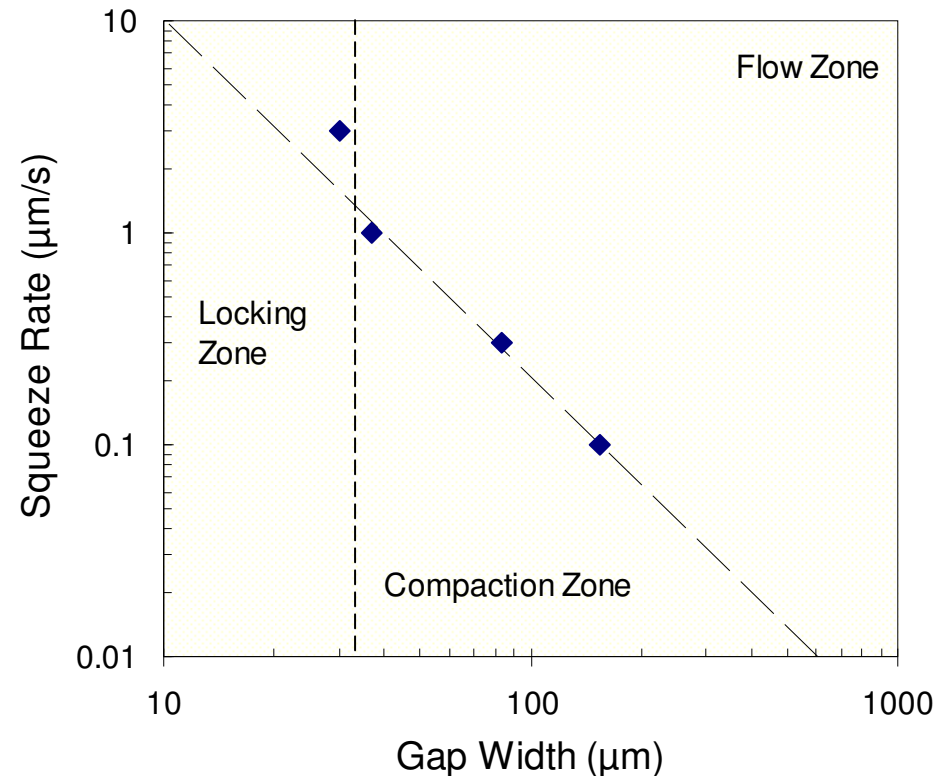
# Exploiting Compaction - Displacement Control



$$\dot{h}_c = \left( \frac{Ak}{\mu_w H^{m+1}} \right)^{1/1-m}$$

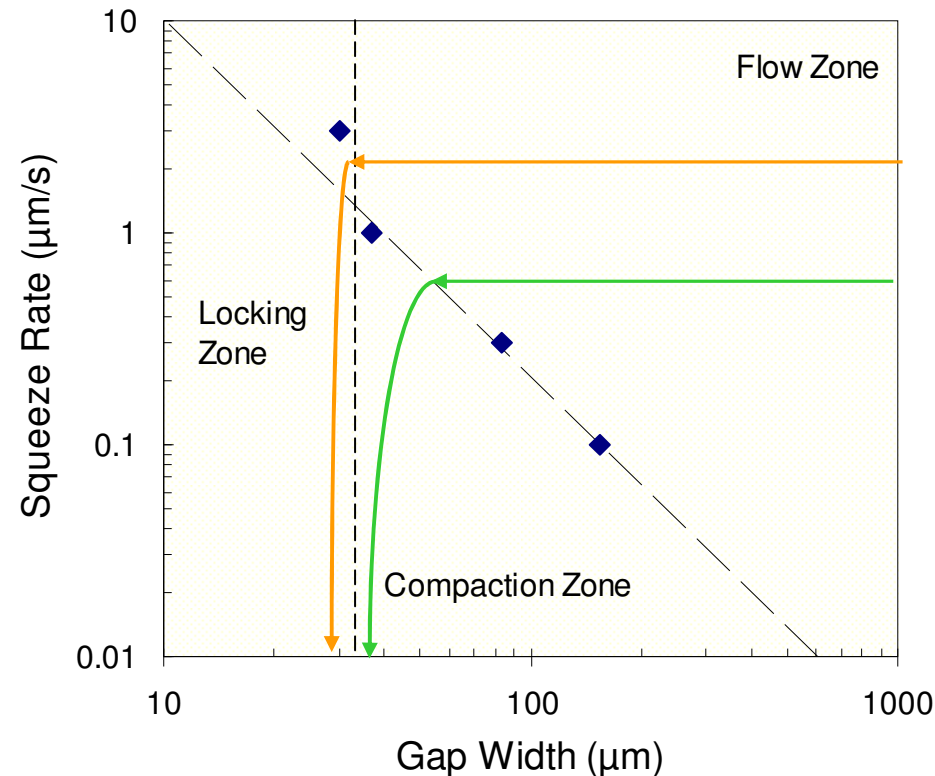
- Bondline thickness (gap width) decreases during processing until the point that the filler particle network supports the load applied
  - For a rapid squeeze, this occurs at several effective particle diameters
  - For a slow squeeze crossing into the filtration zone, this occurs after compaction of the filler network near the stagnation zones

# Squeeze Rate vs. Gap Width Flow Phase Diagram



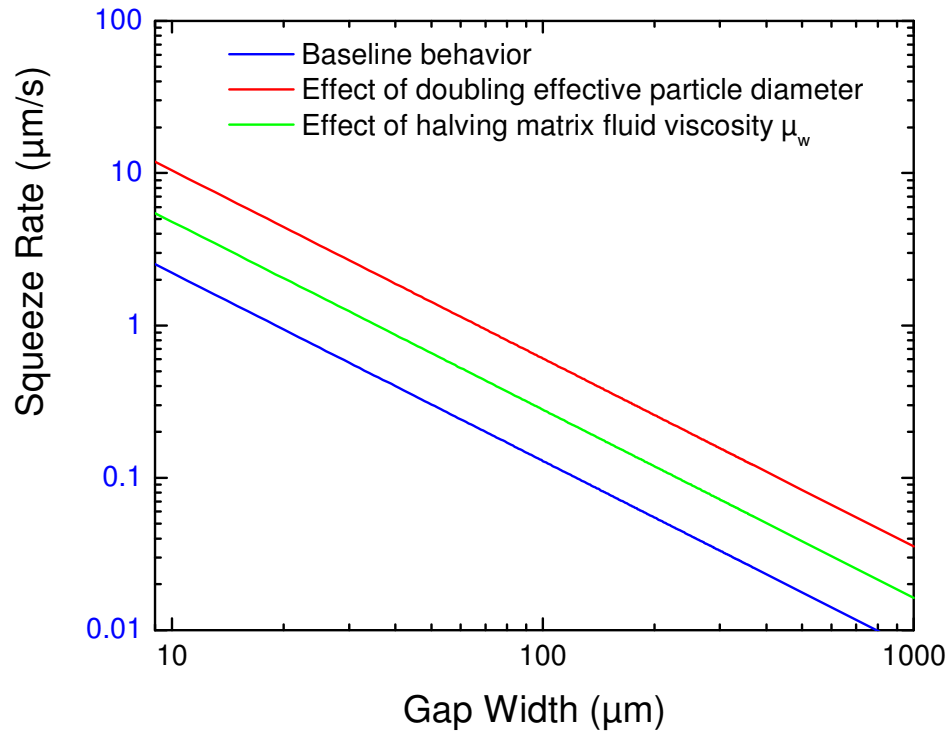
- The critical gap widths trends match well with this description
- If a gap width of several particle diameters is hit without the squeeze rate slowing a bondline with a laterally homogeneous filler distribution will result
- If the process crosses below the critical gap width phase separation line, compaction may occur if the force applied is large enough

# Squeeze Rate vs. Gap Width Flow Phase Diagram



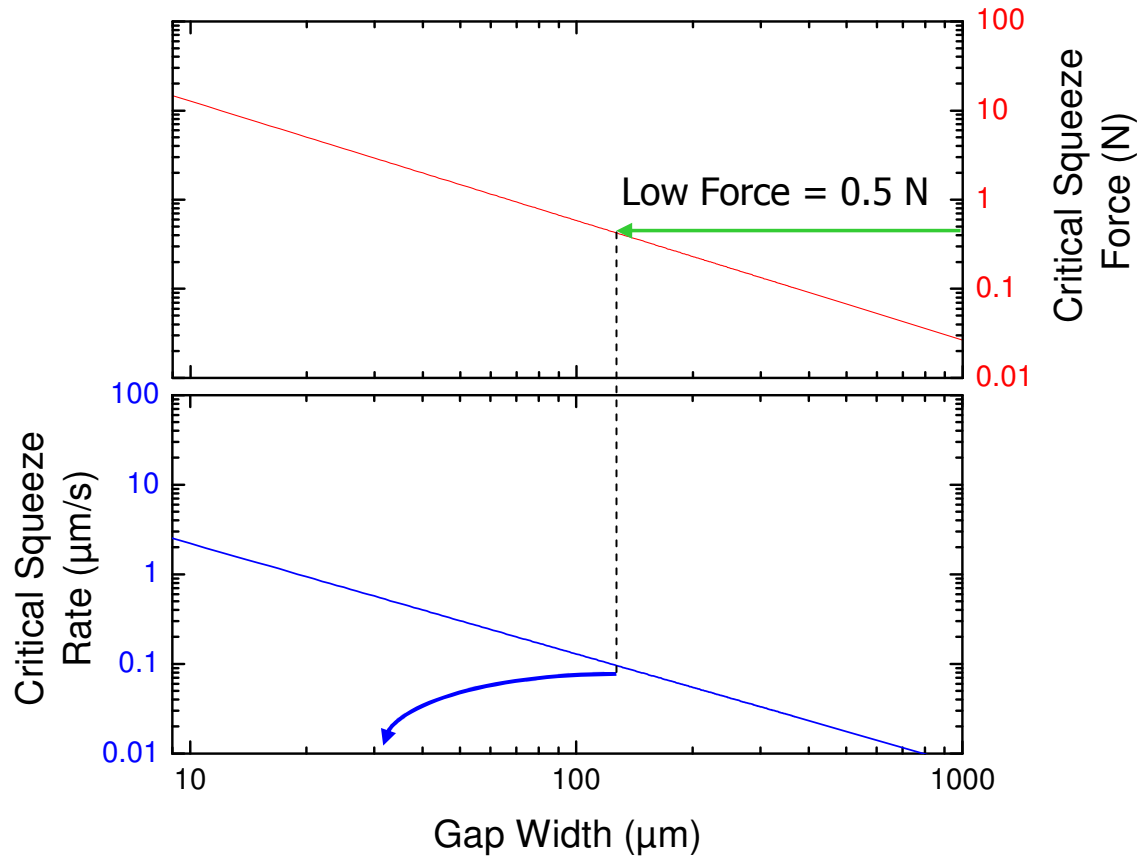
- The critical gap widths trend matches well with this description
- If a gap width of several particle diameters is hit without the squeeze rate slowing a bondline with a laterally homogeneous filler distribution will result
- If the process crosses below the critical gap width phase separation line, compaction may occur if the force applied is large enough

# Potential for Material Development Optimization



$$\dot{h}_c = \left( \frac{Ak}{\mu_w H^{m+1}} \right)^{1/1-m}$$

- This approach allows us to guide the formulation of thermal interface materials to enhance or minimize compaction

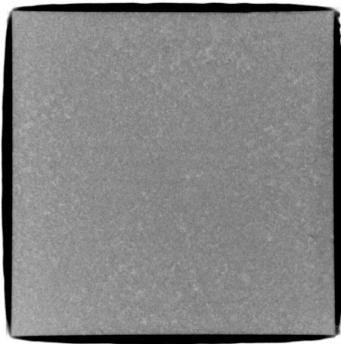
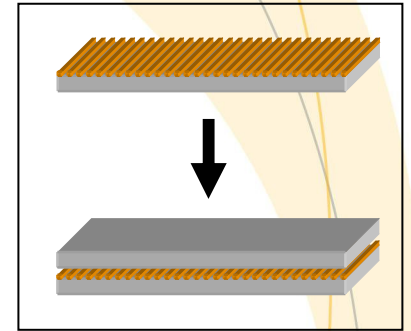
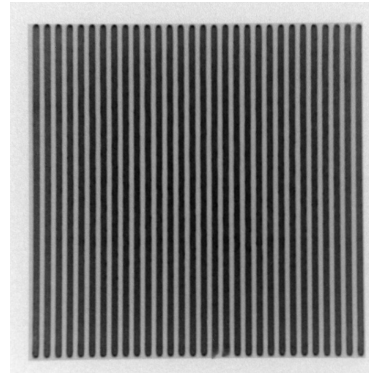


$$F_c = \frac{-\dot{h}_c^m}{H_c^{2m+1}} \left( \frac{2m+1}{2m} \right)^m \frac{\pi k R^{m+3}}{m+3}$$

$$\dot{h}_c = \left( \frac{Ak}{\mu_w H^{m+1}} \right)^{1/1-m}$$

- A critical normal force corresponding to the viscous force of the homogeneous fluid can be calculated for the gap at onset of heterogeneity
- Below this gap, compaction will occur as the squeeze slows

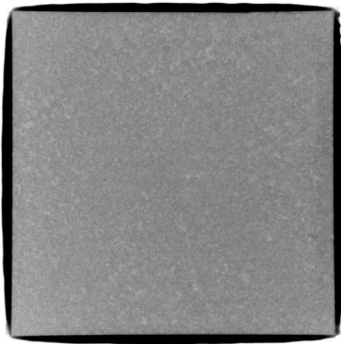
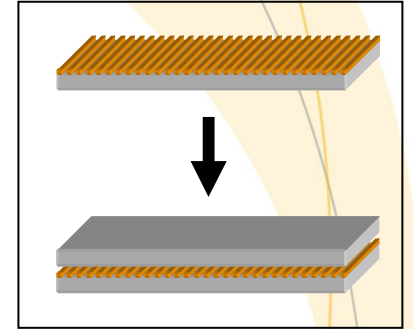
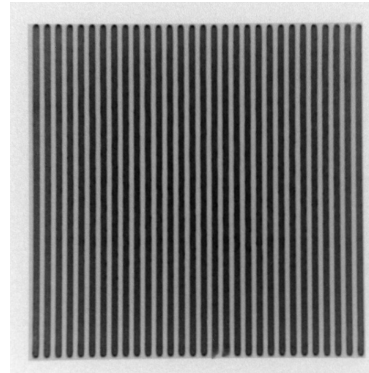
# Visualization of the Effect of Substrate Roughness and Squeeze Rate



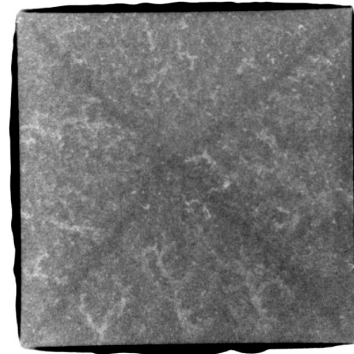
Fast Squeeze Assembly  
Smooth Glass Substrate

**\*X-ray images shown of Si on glass with one of two roughness conditions**

# Visualization of the Effect of Substrate Roughness and Squeeze Rate



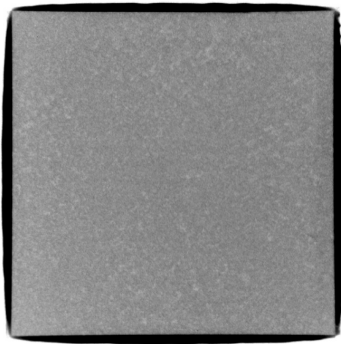
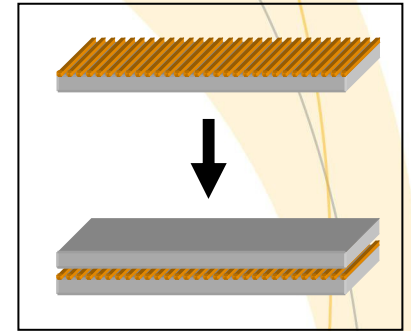
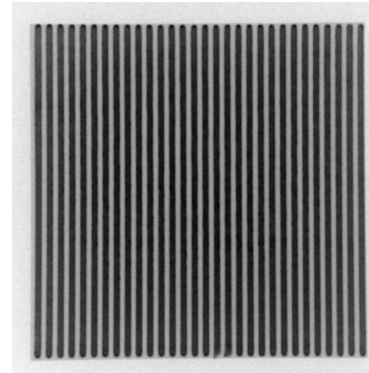
Fast Squeeze Assembly  
Smooth Glass Substrate



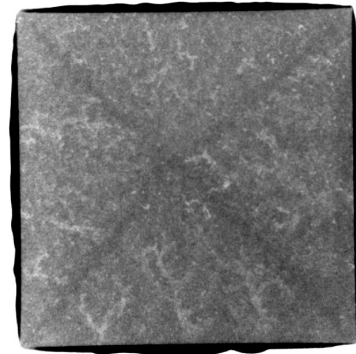
Slow Squeeze Assembly  
Smooth Glass Substrate

**\*X-ray images shown of Si on glass with one of two roughness conditions**

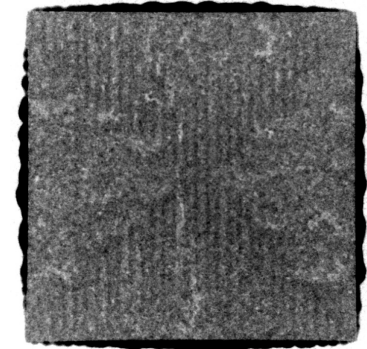
# Visualization of the Effect of Substrate Roughness and Squeeze Rate



Fast Squeeze Assembly  
Smooth Glass Substrate



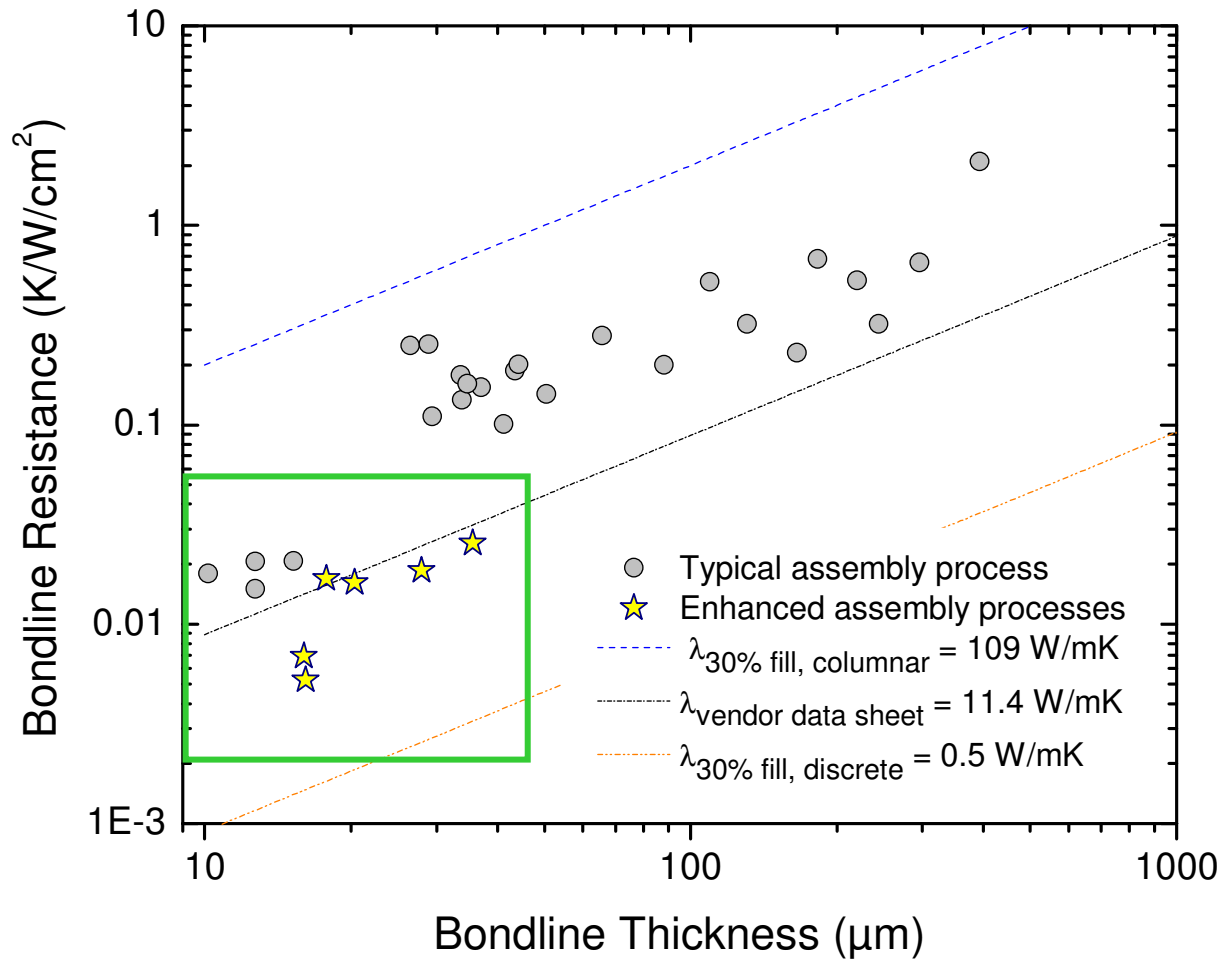
Slow Squeeze Assembly  
Smooth Glass Substrate



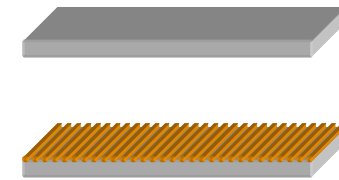
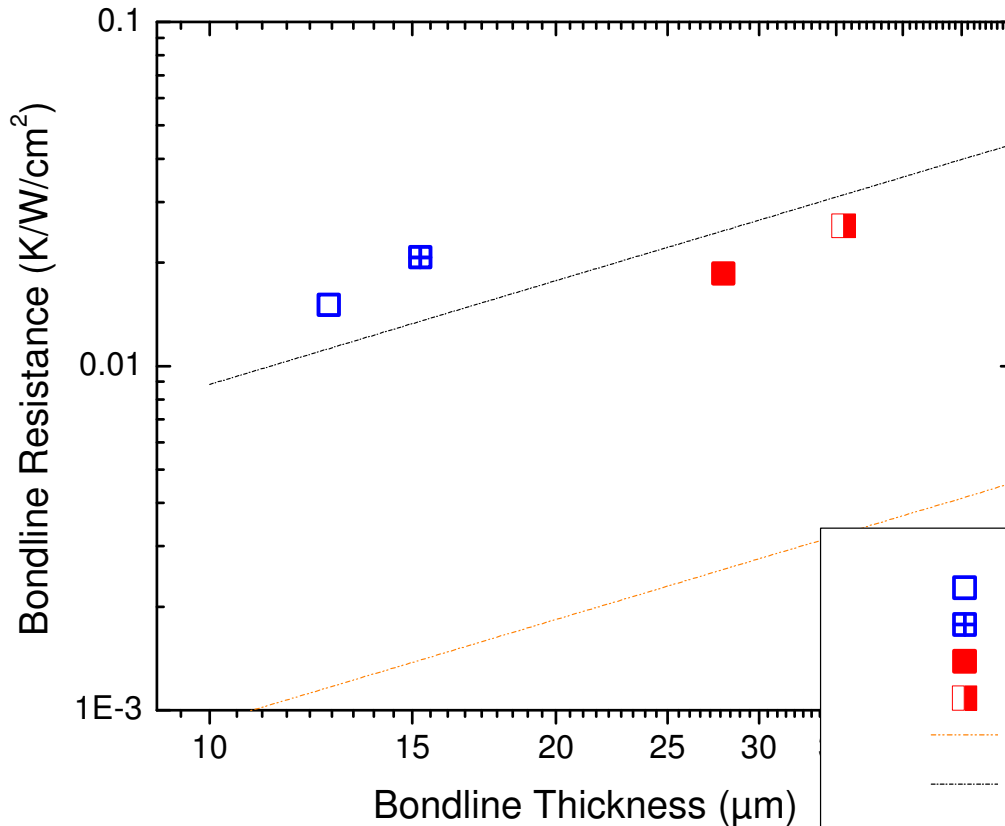
Slow Squeeze Assembly  
Frosted Glass Substrate

**\*X-ray images shown of Si on glass with one of two roughness conditions**

# Thermal Results – All Cured with a Load Applied



# 30 Line Deposit Between Smooth or Rough Square Cu Substrates



- 30 rectangular deposits - smooth - SR 10 µm/s - 100 N
- 30 rectangular deposits - rough - SR 10 µm/s - 100 N
- 30 rectangular deposits - smooth - SR 0.75 µm/s - 100 N
- 30 rectangular deposits - rough - SR 0.75 µm/s - 100 N
- $\lambda_{30\% \text{ fill, columnar}} = 109 \text{ W/mK}$
- $\lambda_{\text{vendor data sheet}} = 11.4 \text{ W/mK}$

- Full gap fill expected at 53 µm
- 10 µm/s squeeze rate – thin bondlines and  $\lambda_{\text{effective}} = 7 \text{ W/mK}$
- 0.75 µm/s squeeze rate – thicker bondlines and  $\lambda_{\text{effective}} = 15 \text{ W/mK}$